

Review

# Separator Materials for Lithium Sulfur Battery—A Review

Ryohei Mori <sup>1,2</sup>

<sup>1</sup> Green Science Alliance Co., Ltd., 2-22-11 Obana, Kawanishi City 666-0015, Hyogo Prefecture, Japan; moriryohai@fuji-pigment.co.jp; Tel.: +81-72-759-8501; Fax: +81-72-759-9008

<sup>2</sup> Fuji Pigment Co., Ltd., 2-23-2 Obana, Kawanishi City 666-0015, Hyogo Prefecture, Japan

**Abstract:** In the recent rechargeable battery industry, lithium sulfur batteries (LSBs) have demonstrated to be a promising candidate battery to serve as the next-generation secondary battery, owing to its enhanced theoretical specific energy, economy, and environmental friendliness. Its inferior cyclability, however, which is primarily due to electrode deterioration caused by the lithium polysulfide shuttle effect, is still a major problem for the real industrial usage of LSBs. The optimization of the separator and functional barrier layer is an effective strategy for remedying these issues. In this article, the current progress based on the classification and modification of functional separators is summarized. We will also describe their working mechanisms as well as the resulting LSB electrochemical properties. In addition, necessary performance for separators will also be mentioned in order to gain optimized LSB performance.

**Keywords:** lithium sulfur battery; rechargeable battery; separator; electrochemistry; anode; cathode

## 1. Introduction

The propagation of modern human society based on the electronic industry has demanded stronger and cheaper energy storage systems. Among these, lithium ion batteries (LIBs) have been aggressively studied and developed because of their high endurance against electrochemistry variation and their stable usage for application in various types of electronic devices, including smart phones, mobile phones, EVs, etc., even though LIBs still suffer from limited capacity, high price, and safety issues, including their flammable nature. Due to these reasons, it would be difficult for LIBs to fulfill the demand for upcoming new industrial applications, such as drones, EVs, military power supplies, and stationary electrical power stations, because they always demand higher capacity as well as safer and economically friendly rechargeable batteries [1–3]. In this regard, lithium sulfur batteries (LSBs) could be one of several alternative candidate rechargeable batteries because of their high theoretical capacity and energy density (1675 mAh g<sup>-1</sup> and 2600 Wh Kg<sup>-1</sup>, respectively). The corresponding values for LIBs are 240–280 mAh g<sup>-1</sup> and 350–400 Wh Kg<sup>-1</sup>, respectively. Apart from the nature of LIBs, the electrochemical reaction of LSBs is different from that of LIBs due to the presence of a sulfur cathode, and can be expressed as:



As a result, LSBs can offer 5–7 times higher energy density than that of LIBs. Combined with its other advantages, i.e., sulfur being naturally abundant, cheap, and a non-toxic element, LSBs can be considered as one of the candidates for next-generation rechargeable batteries [4–7]. The typical configuration of an LSB is shown in Figure 1.

Lithium metal is the anode and a carbon–sulfur composite is the cathode [8]. As an ordinary battery, the separator and an electrolyte exist between the anode and cathode.

When the LSB is discharged, sulfur is reduced to Li<sub>2</sub>S by a series of electrochemical reaction while forming various types of polysulfide intermediates. Figure 2 indicates an ordinary LSB profile during a charge–discharge electrochemical reaction [9].



**Citation:** Mori, R. Separator Materials for Lithium Sulfur Battery—A Review. *Electrochem* **2023**, *4*, 485–522. <https://doi.org/10.3390/electrochem4040032>

Academic Editors: Huang Zhang and Yuan Ma

Received: 14 September 2023

Revised: 22 October 2023

Accepted: 2 November 2023

Published: 13 November 2023



**Copyright:** © 2023 by the author. Licensee MDPI, Basel, Switzerland. This article is an open access article distributed under the terms and conditions of the Creative Commons Attribution (CC BY) license (<https://creativecommons.org/licenses/by/4.0/>).

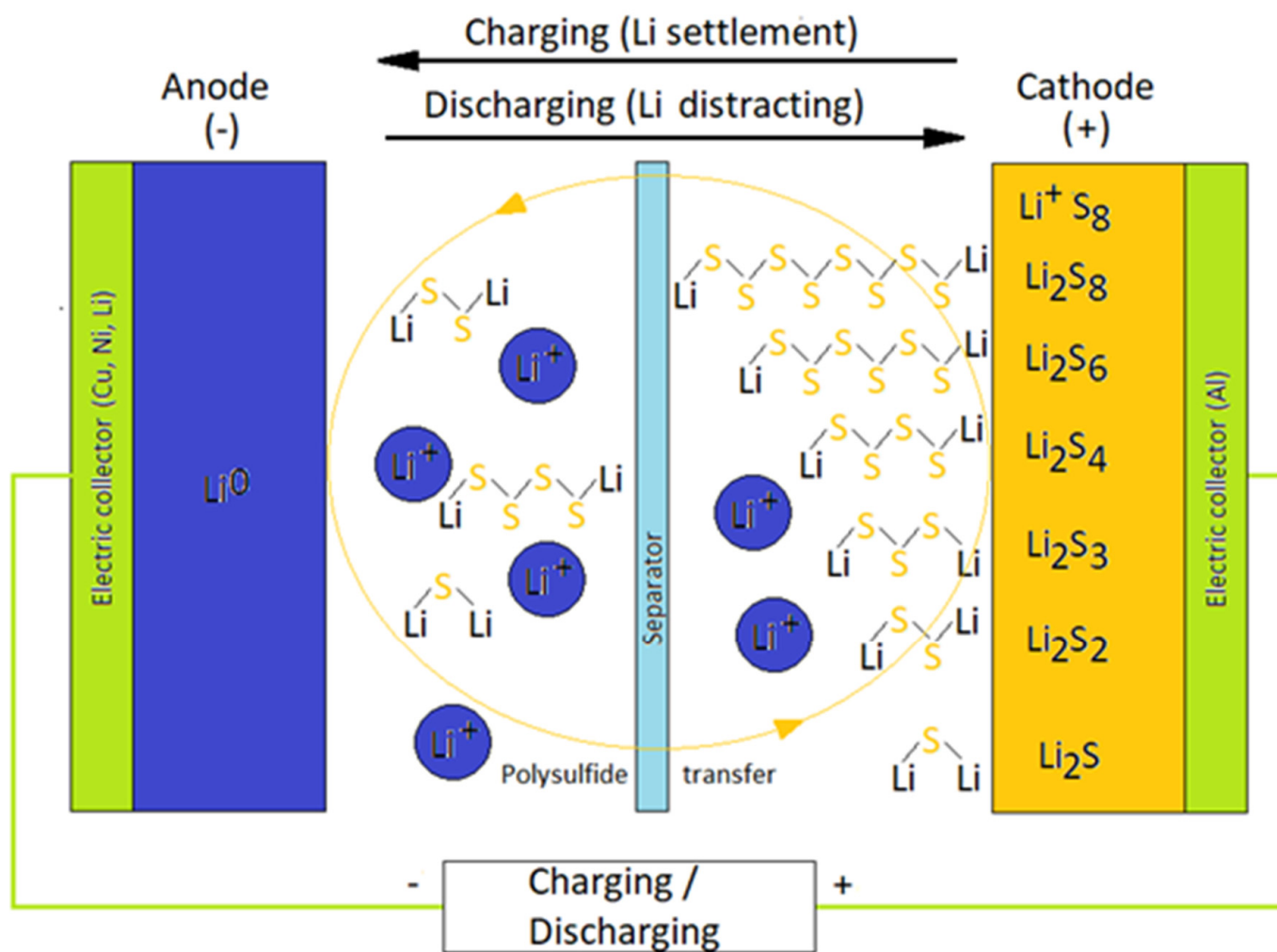


Figure 1. Structure image of LSBs with liquid electrolyte [8].

During the electrochemical reaction, sulfur is reduced to  $\text{Li}_2\text{S}_x$  ( $x = 2-8$ ) via a stepwise electrochemical reaction to form each lithium sulfide compound. The lithium polysulfide (LiPS) compound with a relatively long chain ( $\text{Li}_2\text{S}_x$  ( $x = 4-8$ )) can be highly soluble. On the other hand, the solubility of  $\text{Li}_2\text{S}_x$  ( $x = 2-4$ ) with short chain is lower compared to the long-chained one in the electrolyte [10]. The lithiation of sulfur occurs stepwise. At a voltage of around  $\sim 2.3$  V,  $\text{S}_8$  as the solid state is reduced to soluble  $\text{S}_8^{2-}$  via an initial electrochemical reaction. After that, dissolved  $\text{S}_8^{2-}$  is electrochemically reduced to  $\text{S}_4^{2-}$  on the cathode. During this sequential chemical process, LiPS intermediates such as  $\text{S}_6^{2-}$ ,  $\text{S}_3^{2-}$ , and  $\text{S}_3$  are formed [11,12].

As LiPS concentration increases gradually throughout the electrochemical reaction, the viscosity of the electrolyte is enhanced. Gradual voltage decrease can be seen at this stage of reaction. After these events, one can observe a prolonged voltage of around 2.0–2.2 V, which is the major origin of LSB capacity. During this stage, an electrochemical reaction, which transforms soluble low-ordered LiPS to insoluble  $\text{Li}_2\text{S}_2$  or  $\text{Li}_2\text{S}$ , takes place.

At the final stage,  $\text{Li}_2\text{S}_2$  would become  $\text{Li}_2\text{S}$  via a reduction process. However, it should be noted that since this is the solid–solid phase reaction, the kinetics are slow due to sluggish ion diffusion. The insulating characteristics of both  $\text{Li}_2\text{S}_2$  and  $\text{Li}_2\text{S}$  are an additional cause for a slow electrochemical reductive reaction [13].

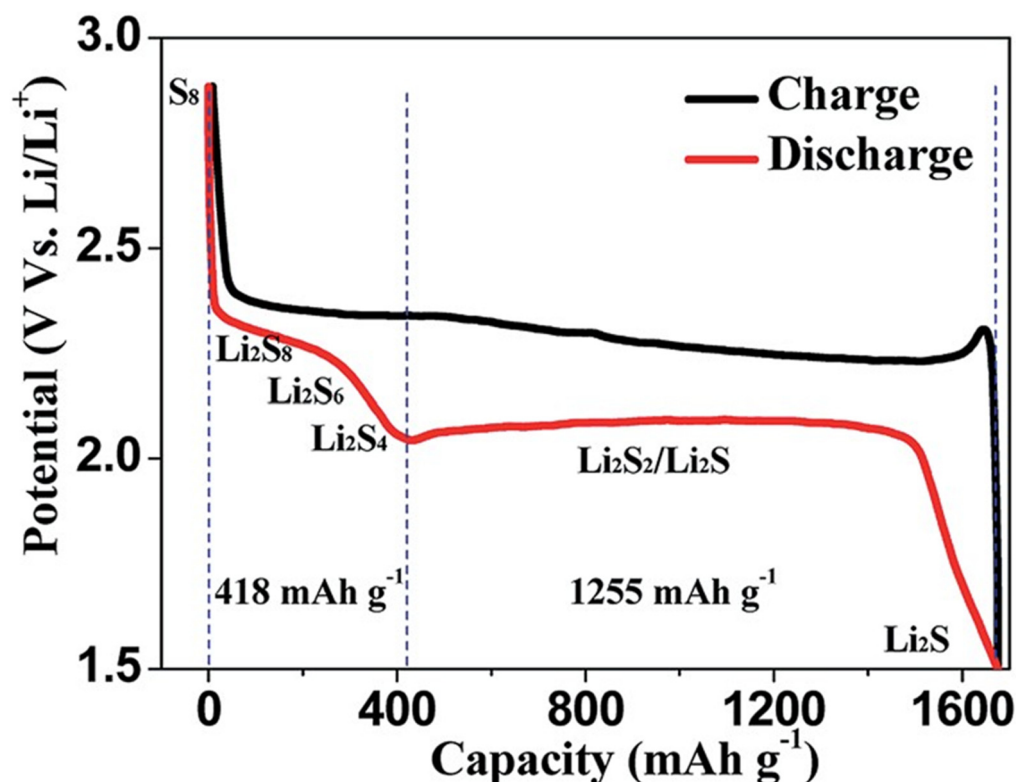


Figure 2. An ordinary charge/discharge profile curve for LSBs [9].

In spite of these advantages, LSBs still face with obstacles for practical industrial usage. For example, sulfur as a cathode active material has insulating characteristics for both the electron and the ion. LiPS as byproducts are formed in the liquid electrolyte (shuttle effect) during the discharge process, which reduce the mass and utilization of cathode sulfur. In addition, the dendrite formation of a lithium anode may cause fire once they reach the other side of the electrode through a state of battery short circuit. Furthermore, volume expansion induced by the electrochemical reaction of S to  $\text{Li}_2\text{S}$  would result in losing stability in the cathode structure [14,15].

A tremendous amount of effort has been carried out to overcome these problematic issues by increasing the cathode materials' conductivity as well as by reducing LiPS dissolution in the electrolyte [16–19]. For example, an increase in conductivity in the cathode structure is being attempted by researchers by applying conductive carbon, carbon nanotube, graphene, as well as conductive polymer. To prevent LiPS dissolution in the electrolyte, various kinds of oxides, sulfides, nitrides, and carbides, alongside some functional materials such as quantum dot and a metal organic framework, have been replaced with carbon to reduce the shuttle effect [20–23].

Further challenges facing the cathode and electrolyte development for LSBs have been recently accelerated due to the strong influence upon the electrochemical properties. The key function of an LSB electrolyte is to transport  $\text{Li}^+$  ions in the battery efficiently, and this requires a high level of  $\text{Li}^+$  conductivity. The composition of electrolyte also largely influences the cathode electrode reaction as well as the behavior of LiPS byproducts [24–26].

In addition to designing cathodes and electrolytes, a separator is also a critical LSB component to effect its performance, especially in terms of suppressing the LiPS problem as separators can be reservoirs or capturing materials for polysulfide intermediates. Additionally, when separators have conductivity, for example, they can behave as the second current collector for electrons, which would result in enhancing the LSB electrochemical performance [27]. Nevertheless, it should be mentioned here that any additional separator

weight due to modifications should be carefully regulated to maintain the battery energy density as a whole [28].

In general, polypropylene (PP) and polyethylene (PE) are utilized as separators, although it would be difficult for these nonpolar and hydrophobic materials to suppress the LiPS shuttle effect, because lithium polysulfide is more polar in nature [29]. As a preparation procedure, direct coating, slurry coating, or the filtration of functional materials onto a commercial separator would be enough to make such separators in order to prevent the LiPS shuttle effect. Besides LiPS suppression, such functional separators are also expected to possess catalytic activity and good mechanical strength for LSBs [30].

Fortunately, this kind of process, such as the direct coating of functional materials which ink or slurry onto the separator, can be applied to an industrial manufacturing process easily. In particular, important parameters, including thickness, weight, size, and the kind of functional materials on a separator, can be readily controlled and applied to real practical industrial processes, even though sulfur, as an active material, is essentially an electrical insulator, and so it needs to be encapsulated in a conductive carbon matrix to provide appropriate electronic contact.

Furthermore, it is necessary to provide ionic pathways through the entire cathode to ensure the conversion reaction between the sulfur and lithium ions. Thus, intimate contact and particle distribution among the carbon, sulfur, and additives is a critical factor. On top of that, the practical slurry manufacturing of actual pouch cell mass production is still challenging. In this regard, Kaskel et al. introduced the ball milling procedure for a scalable preparation method in order to achieve high sulfur utilization and loading. They clarified the carbon/sulfur agglomeration breakdown, decreasing particle size, suitable pore size volume, and distribution, which resulted in enhancing the electrical conductivity of the carbon/sulfur composite as well as achieving a higher electrochemical performance [31]. Similar studies of an improved electrochemical performance by introducing the high-energy ball milling method can be found in some other literature works [32,33]. Younes also investigated the aggregation process between carbon nanomaterials and metal oxide particles, and improved the dispersion status in aqueous solutions [34].

Since commercial separators possess a hydrophobic nature in general as explained above, it is more ideal to use hydrophilic materials to capture LiPS and prevent the shuttle effect. The thickness, weight, as well as porosity of functional layers on separators also need to be taken into consideration because they directly influence the rate of electrons and lithium ions, as well as liquid electrolyte uptake [35].

One has to also consider the modified separators: whether they are either facing the anode or cathode side. This is because the separator's role is largely influential, depending on whether they are placed toward the anode or the cathode direction. Although the main issue with LSBs is the shuttle effect induced by LiPS, lithium dendrite growth during the electrochemical process is another problematic issue. Lithium metal dendrites are formed by a side chemical process between polysulfide and lithium metal. Thus, functional interlayers on the anode side could be one of the possible solutions to prevent dendrite growth by placing the internal layer at the extra space on the anode side. This kind of interlayer may act as a second barrier layer against any leaked LiPS from the cathode side, as well as preventing dendrite physical puncture to the separator. In addition, a functional interlayer or separator could decrease the interfacial resistance of metallic lithium anode by introducing a lithium compatible material. An anode-facing functional separator may also act as the scaffold for lithium ion in order to suppress lithium dendrite growth [36].

Compared with cathode-facing separators, anode-facing separators should have a somewhat lithiophilic nature, endowing them with a high compatibility with lithium metal, in addition to their ability to functionally suppress the shuttle effect. This will control the spatial distribution of lithium deposition during redox reactions. When these properties are optimized, they can be expected to more efficiently hinder the dendritic growth of the lithium metal [37].

The remainder of this paper will explain: whether the functional layers or separators face the anode or cathode side; the material classifications of separators and their working mechanisms; and the electrochemical properties of the resulting corresponding assembled LSB. The separator materials which we have selected for this review are as follows.

## 2. Separators Classified by Materials

### 2.1. Separator Material Facing Anode Side

#### 2.1.1. Separator Material: Metal

Nanoparticle- or nanolayer-based materials can inhibit dendritic Li growth by controlling lithium nucleation [38]. The nanoparticles in anode-facing separators behave as nucleation sites for lithium metal during electrochemical reactions as they decrease the Gibbs free energy of lithium metal electrodeposition. Initially, lithium crystal seeds would gradually grow until they cover the entire surface of the separator surface. As the process proceeds, dense lithium metal layers without dendrites are formed on the separator. Liu et al. demonstrated this phenomenon by applying lithiophilic Mg nanoparticles to an anode, whereby an LSB was prepared with this unique functional separator and which exhibited high-capacity retention (>80% after 400 cycles) [39]. Furthermore, the morphology of nanoparticles can confer the cathode structure with appropriate pores and voids, which could be a favorable lithium ion transportation channel to enhance LSB electrochemical performance. It should be noted here that Mg, Ag, and Au are also known to lower the Gibbs free energy of lithium electrodeposition.

Zuo et al. investigated the Li metal deposition phenomenon in a symmetrical cell system. As a result, lithium dendrites were seen on the surface of the pristine Li metal anode after an electrochemical discharge process, as confirmed and shown in Figure 3a. When Ag was co-deposited, Li dendrites had a tendency to fill the interspace among the Ag particles, which resulted in a lateral growth (Figure 3b). When the cross-sectional SEM image was observed, without Ag introduction, clear Li dendrites were seen after 50 cycles of the electrochemical charge–discharge process (Figure 3c). When Ag was introduced to the Li metal, in contrast, the electrode surface with a dense Ag–Li alloy layer without any Li dendrites was observed (Figure 3d). This surprising Li-dendrite-suppression effect of Ag introduction to the Li metal anode was suggested to be due to the strong affinity of Li with Ag metal. We would like to look at one example of LIB apart from LSB. With this interesting mechanism, Li ions were deposited uniformly during an electrochemical charge–discharge process. As a result, when  $\text{LiFePO}_4 \mid \text{Li}$  full cell was prepared with Ag, introducing the Li metal as anode, it exhibited a  $131 \text{ mAh g}^{-1}$  capacity, even after 300 cycles [40]. Not only was a metal material introduced, but copper was also functionalized to the lithium metal anode to prepare a 3D Cu/Li and copper mesh/Li composite anode. Yang et al. clarified that Li dendrite growth was successfully suppressed with a 3D Cu/Li-structured anode, which can operate for 600 h and demonstrated low voltage hysteresis [41,42].

#### 2.1.2. Separator Material: Ceramic

Boron nitride was applied to optimize the commercial separators, owing to its intrinsic high levels of insulation and high thermal conductivity [43]. Boron nitride (BN)/carbon-modified composite separator was prepared with a coating method on a separator. Figure 4A shows a schematic figure and the functions of the BN/carbon separator in an LSB. During discharge, LiPS spreads out from the sulfur cathode toward the lithium anode metal. The carbon layer hinders the diffusion of the LiPS acting as the first blocking layer, and any LiPS that diffuses through the carbon layer is subsequently trapped by the BN layer acting as the second blocking layer. This BN/carbon separator was made by direct ink casting (ink composed of carbon nanopowder and BN nanopowder) onto a polypropylene separator via the slurry coating method. Owing to this simple procedure, large-scale separator fabrication (dimensions 150 mm long and 60 mm wide) could be achieved (Figure 4B). The prepared separator had sufficient mechanical strength and was able to resist physical twisting due to the strong level of adhesion between the separator, carbon, and BN nanopowders, having

been bonded using a polyvinylidene fluoride (PVDF) binder (Figure 4C). Figure 4D shows the surface of a pristine commercial polypropylene separator, on which some distributed pores can be observed. After coating the separator with BN (particle size  $\sim 100$  nm; Figure 4E) and carbon (particle size  $\sim 50$  nm; Figure 4F) nanopowders, the pores were fully covered. BN and the carbon layer thickness were approximately 7 and 6  $\mu\text{m}$ , respectively (Figure 4G). Some of the electrochemical properties of the prepared LSBs were measured. After the surface modification, lithium dendrite formation was suppressed by forming on the Li surface by an ideal Li plating/stripping process (Figure 4H). Fortunately, LiPS diffusion was mitigated by an additional BN layer on the separator, thus resulting in obtaining a higher LSB electrochemical performance (Figure 4I) [43].

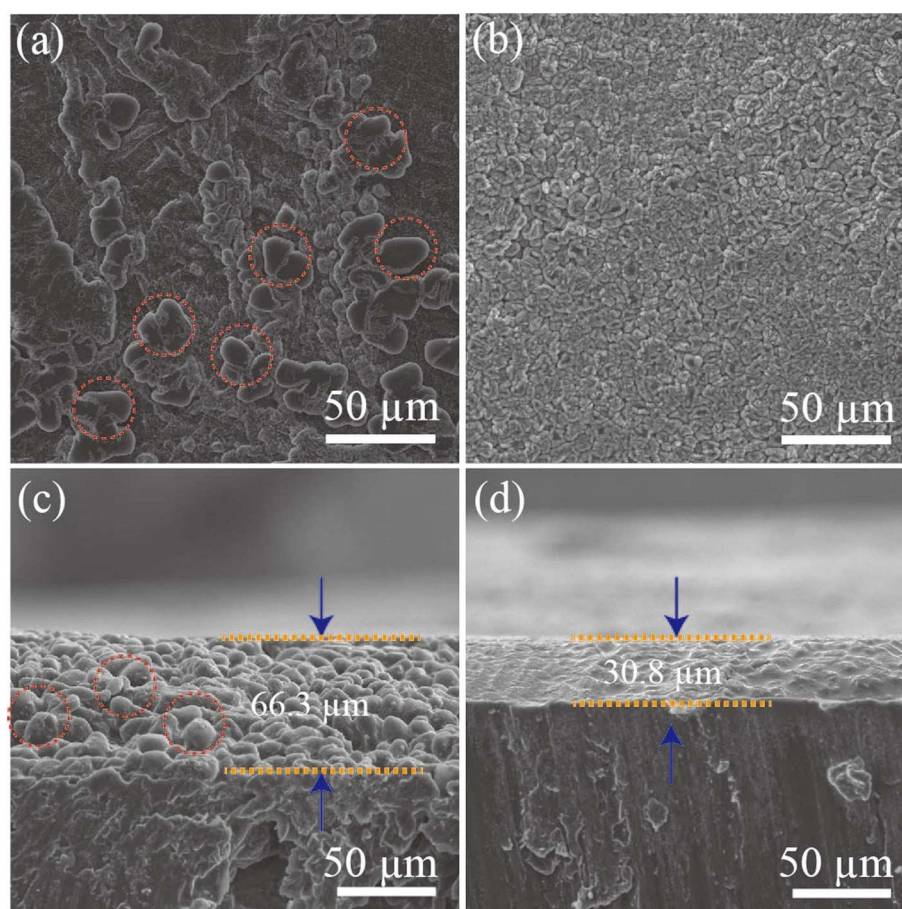


**Figure 3.** Surface observation: (a) bare lithium; (b) Ag co-deposited lithium with SEM. SEM observation of cross-sectional (c) bare lithium; (d) Ag co-deposited lithium [40].

In addition to controlling the lithium metal growth and nucleation, the oxide functional interlayer could also be ideal in suppressing the LiPS effect. Silica ( $\text{SiO}_2$ ) is one such material effective for preventing the LiPS shuttle effect and improving LSB performance. One of its advantages is its abundance. The thermal stability of  $\text{SiO}_2$  is also a good feature in order to confer the separator with high thermal stability [44]. However, its direct contact with the cathode should be prevented as  $\text{SiO}_2$  is known to react with lithium metal [45]. However, it should be noted that one of the  $\text{SiO}_2$ -coated separator example will be presented in a later section. In addition,  $\text{SiO}_2$  has high affinity with LiPS, making it suitable for suppressing the LiPS shuttle effect [46]. Therefore,  $\text{SiO}_2$  utilization as functional LBS separators could be one of several effective methods. Li et al. attempted an  $\text{SiO}_2$  coating of a polypropylene (PP) separator using the tetraethoxysilane (TEOS)-based sol-gel method. They have elucidated that by applying PP- $\text{SiO}_2$  separator, wettability and thermal stability were properly improved. As a result, rate and cyclic voltammetry performance improved,

owing to suppressed LiPS shuttle effect as well as promoting lithium ion transport inside LSBs [47].

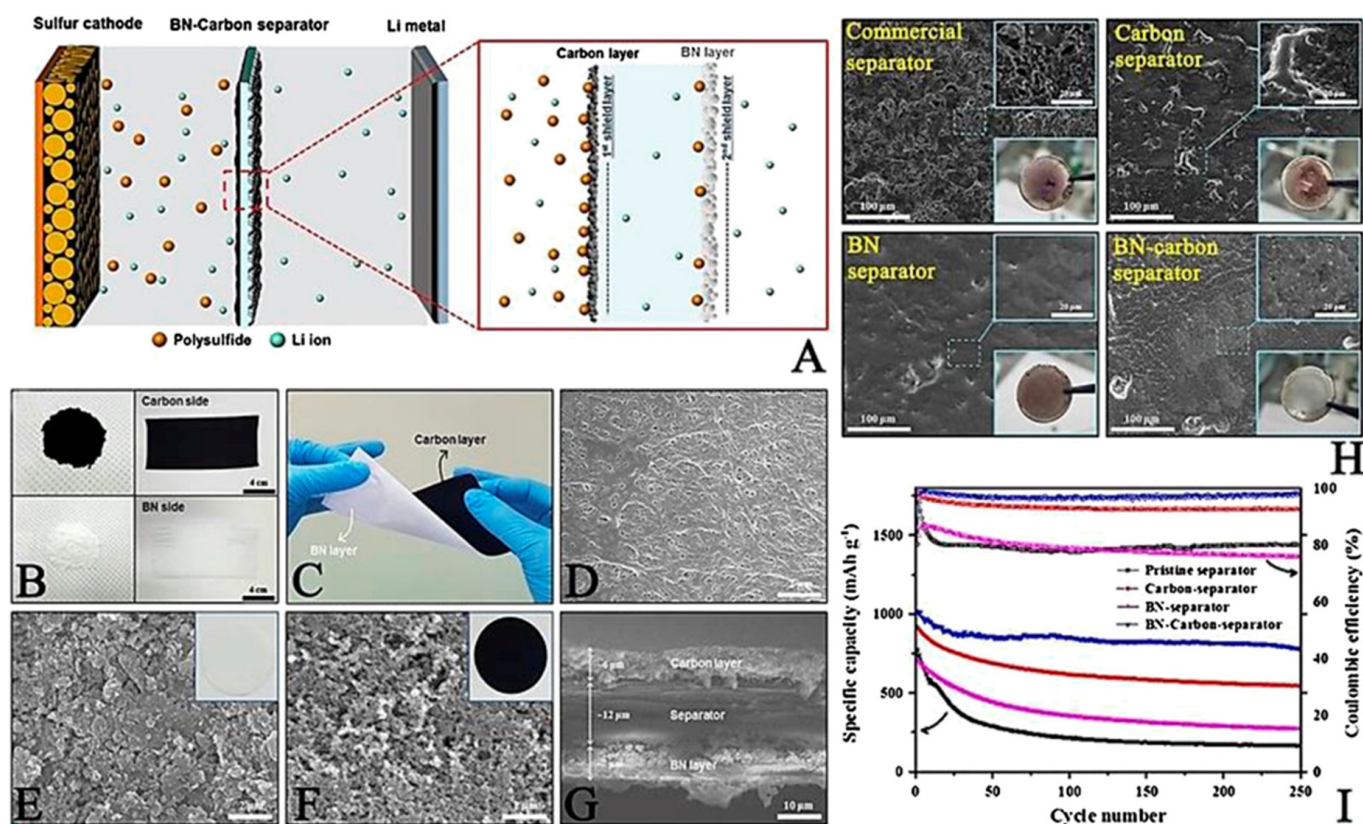


**Figure 4.** (A) Speculated image of the BN-carbon separator role. (B) Separator of BN coating layer. (C) Bent BN-coated separator image. Top view of SEM image of (D) intact separator. (E) BN side separator. (F) Carbon side of a BN-carbon separator. (G) Cross-sectional SEM view of a BN-carbon separator. (H) Photographs of a lithium metal anode of LSB prepared with described type of separators in each picture, after 250 cycles. (I) Cycle performances of various kinds of separators at 0.5 C [43].

The chemical stability and LiPS adsorption ability of alumina ( $\text{Al}_2\text{O}_3$ ) are relatively high. Hou et al. elucidated that the oxygen atom with a lone electron pair of oxide materials such as  $\text{Al}_2\text{O}_3$  and  $\text{SiO}_2$  has strong dipole-dipole interactions with LiPS [48]. Wang et al. prepared a purely inorganic separator with  $\text{Al}_2\text{O}_3$  nanowires. In general, a purely inorganic separator without any base organic polymer would have a brittleness problem compared to conventional organic PP separators, whereas the advantages of a ceramic separator are a higher uptake of liquid electrolyte and higher porosity. They often also exhibit improved thermal stability and enhanced conductivity compared to the organic ones. This mechanism can be applied not only for LSBs, but also LIBs. For example, when an alumina separator was applied for  $\text{Li} \parallel \text{LiFePO}_4$  (LFP), the battery electrochemical characteristics were better than a conventional PP separator-based battery [49].

Regarding LSB, He et al. prepared an  $\text{Al}_2\text{O}_3$  thin film on a commercial separator on the anode-facing side in order to examine the lithium dendrite formation prevention effect. It was found that the  $\text{Al}_2\text{O}_3$  layer successfully mitigated the chemical reactions between LiPS and the lithium anode. They also discovered that the porous structure of the prepared  $\text{Al}_2\text{O}_3$  accelerated uniform lithium nucleation, which resulted in preventing lithium dendrite growth to form a smooth and dense lithium anode [50].

### 2.1.3. Separator Material: Solid Electrolyte

$\text{Li}_{6.4}\text{La}_3\text{Zr}_{1.4}\text{Ta}_{0.6}\text{O}_{12}$  (LLZTO) is the lithium ion conductive solid electrolyte, and it was coated on the PP separator on the anode side. Smooth lithium deposition was achieved due to a uniformly dispersed transportation path for the lithium ion in three-dimensional structure in LLZTO. It was also clarified that lithium ion deposition was further enhanced by adding a higher content of LLZTO by localizing a higher content of anions. Owing to these improvements, the prepared LSB presented an improved electrochemical performance with better safety due to solid electrolyte stability [51].

### 2.1.4. Other Functional Separator Materials

As we have seen above, a modified anode-facing separator could act as a simple barrier to push back LiPS immigration from the cathode to the anode, and this would also be expected to impede Li dendrite formation. For example, there is a kind of conducting polymer that is known to capture LiPS, promoting Li ion flux and electron transportation. Li et al. prepared a conductive polypyrrole (PPy) film for a commercial anode-facing separator and succeeded in improving LSB electrochemical properties [52]. They deposited the PPy film on the separator by applying an Fe-based precursor and pyrrole monomer and succeeded in obtaining a PPy-modified separator (Figure 5a,b). A scanning electron microscope (SEM) observation of the pristine commercial separator exposed 100–200 nm sized nanopores (Figure 5c). In contrast, slightly smaller nanopores with sizes of 30–50 nm were observed on the PPy-coated separator (Figure 5d). The thickness and weight of the coated PPy layer were as small as 15–25 nm and  $\sim 0.13 \text{ mg cm}^{-2}$ , respectively, which is advantageous for industrial use in terms of energy density per weight (Figure 5e). X-ray photoelectron spectroscopy (XPS) was carried out upon both separators. We have observed a peak at 399.8 eV, which can be ascribed to N 1s with the PPy-coated separator (Figure 5f). Nitrogen-originated peaks, including  $-\text{N}=\text{}$  (399.6 eV),  $-\text{N}-$  (400.7 eV), and  $\text{N}^+$  (401.7 eV), are observed from PPy [53,54]. From these spectra results, we suggest that the hydrophilicity of PPy is effective in capturing and suppressing LiPS from the shuttle effect [55,56]. PPy also chemically adsorbed LiPS, owing to its special structure and functional group. As a result, Li dendrite formation was suppressed by the enhancement of the homogenous Li ionic flux and Li plating/stripping.

Preparing a physical barrier by introducing some kinds of lithium compound to a separator is an alternative way to reduce the unfavorable reactions between LiPS and lithium metal. This concept is different from using a material that would not react with any LSB component. Based on this concept, the lithium compound, LiF, was applied to a separator. Lewis acid lithium atoms in LiF could relate with 1,2-dimethoxyethane (DME) as Lewis alkali to form LiF–DME clusters. These clusters are viscous sol and form dense layers that would behave as a shield to prevent the shuttle effect of LiPS. Li et al. utilized this method to improve the electrochemical properties of LSBs [57].

Cathode-facing functional separators could also be effective as anode-facing counterparts because they can serve as the first barrier to LiPS, potentially increasing the chances of sulfur utilization as an active material. To date, polymers, metal compounds, ceramics, carbonaceous material, and their composites have been used to alter commercial separators in order to endow them with additional positive properties [58]. Separators should be mechanically strong, chemically and electrochemically stable, and lightweight in order to avoid negatively impacting the density of energy of the final LSB product. Furthermore, they should possess an enhanced ionic conductivity and the ability to suppress the shuttle effect of LiPS. The functions of a cathode-facing separator can be generally classified as physical adsorption, chemical adsorption, catalytic conversion, and dual-mechanism functions, as shown in Figure 6 [35].

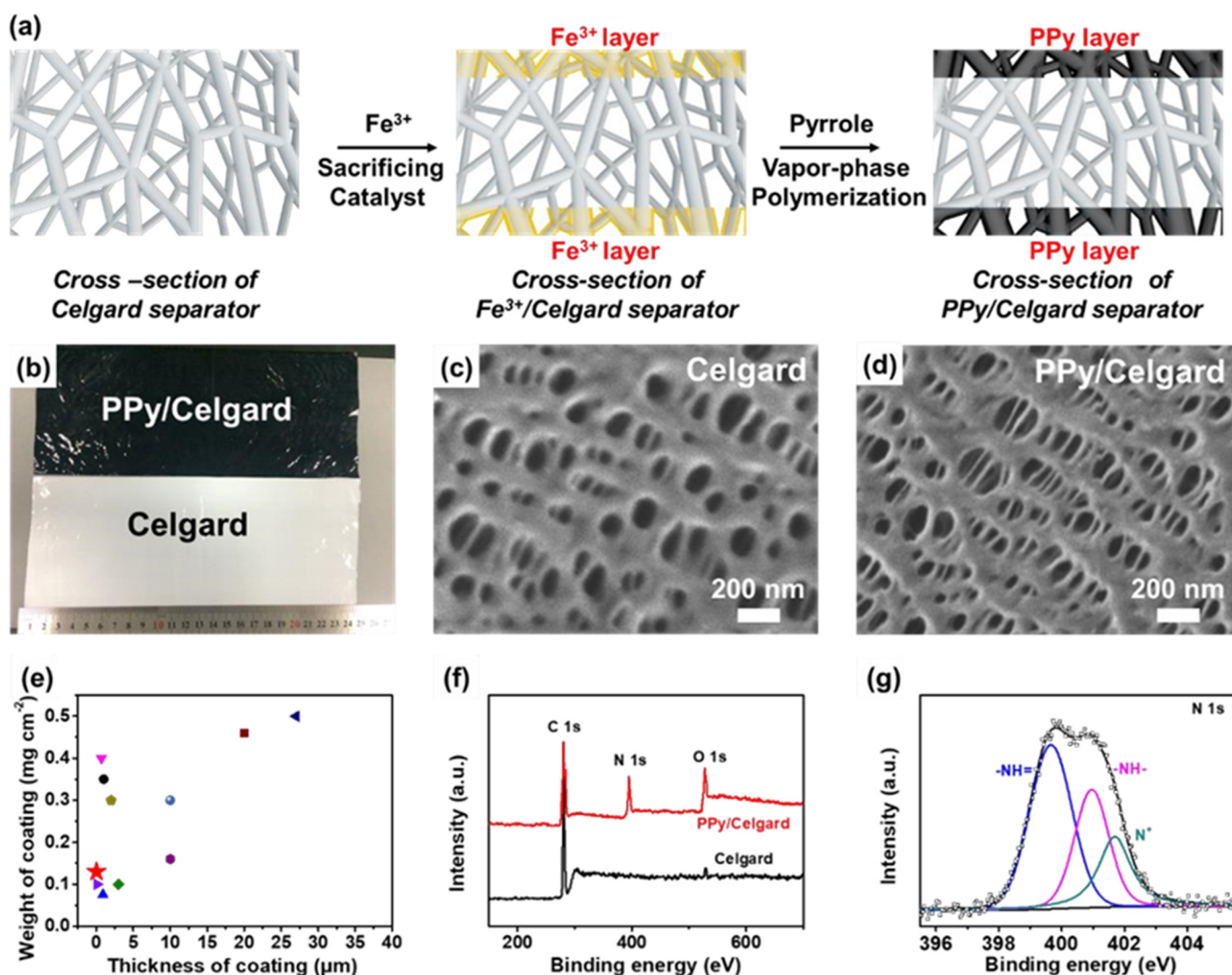


**Figure 5.** (a) The speculated image of PPy layer on a commercial separator by a vapor-phase polymerization method. (b) Actual image of commercial separator with and without PPy treatment. SEM image of commercial separator (c) without and (d) with PPy treatment. (e) Comparison and other examples of the weight and thickness with various types of coating in this work and previous studies. (f) XPS spectra of a separator with and without PPy treatment. The spectrum of N is originated from the PPy-treated layer. (g) Expanded N 1s spectrum of the separator with PPy treatment [52].

## 2.2. Separator Material Facing Cathode Side

### 2.2.1. Separator Material: Carbonaceous Materials

Commercial separators are composed primarily of PP and PE and are considered to be purely physical barriers. In light of this, a great number of research were carried out to study the influence of applying carbonaceous material to the cathode side of the separator, owing to its high electrical conductivity. These carbonaceous materials, including conductive carbon black, carbon nanotube, and graphene, are being studied with an aim to enhance LiPS suppression, cycle stability, and capacity of LSBs [59,60]. The improved electrochemical characteristics of LSBs are mainly the result of high electrical conductivity, which can confer them to behave as additional current collectors to lower the battery resistance [61]. In addition, a sulfur cathode-facing carbon-loaded separator would act as an obstacle to suppress the shuttle effect of LiPS.

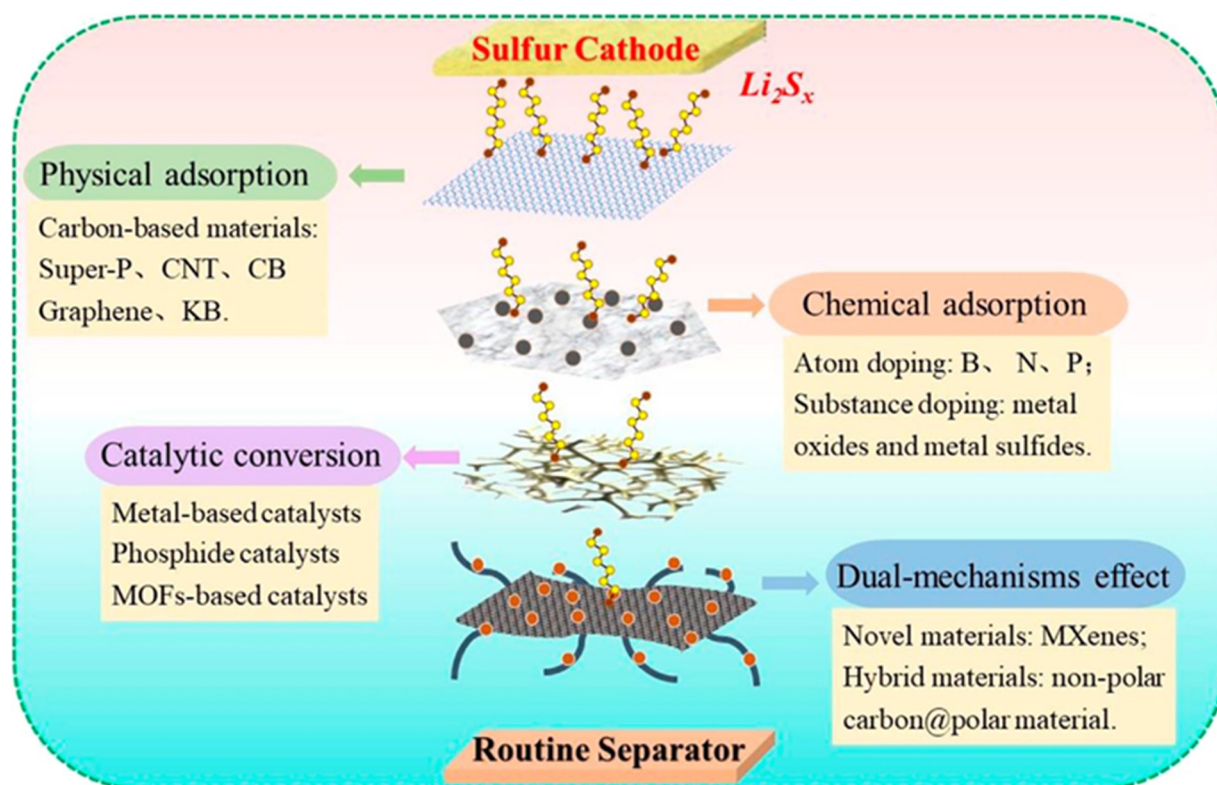


**Figure 6.** Classification and functional mechanism of functional separators in LSBs [35].

For example, eight separators coated with the conducted carbon of various porosities were investigated by Huang et al. to see how the material characteristics contributed to LSB separator performance [62]. The LSB with the nonporous carbon-loaded separator demonstrated a  $1112 \text{ mAh g}^{-1}$  capacity at a C/10 cycling rate, and even after 200 cycles, a stable reversible capacity of  $710 \text{ mAh g}^{-1}$  was maintained [63].

Kim et al. prepared a separator treated with carbon nanotubes conjugated with hydroxyl groups. The experimental results and theoretical calculation confirmed that the hydroxyl groups on carbon nanotube surface promoted good LiPS-capturing effect on the cathode side. Furthermore, the LiPS migration decrease to the anode side conferred the lithium electrode with good stability. In addition, the high conductivity of carbon nanotube with hydroxyl group assisted in the reuse of adsorbed intermediates for further electrochemical reaction (Figure 7). Because of these efforts, the prepared LSB demonstrated  $1056 \text{ mAh g}^{-1}$  at the beginning and a capacity fading rate of 0.11% per cycle over 400 cycles at a 0.5 C rate [63].

Besides conductive carbon and carbon nanotubes, graphene can be also considered as an attractive functional coated material to improve the separator properties. In general, graphene possesses high electrical conductivity, is super lightweight, has high chemical stability and ductility, and is mechanically strong. The separator coated with graphene blocks pores in the polyolefin separator, which can prevent LiPS dissipation. Reduced graphene oxide (rGO) was obtained using Hammer's method, and it was dispersed in DMF (dimethylformamide) and combined with sodium ligno-sulfonate (SL) and hexamethylene diisocyanate (HDI). SL is rich in hydroxyl, carboxyl, and dendritic groups and it is considered an industrially cheap and available material. IR spectra elucidated a broad peak at  $3400 \text{ cm}^{-1}$ , which can be ascribed to stretching vibrations of the hydroxyl group, and  $1634 \text{ cm}^{-1}$ ,  $1402 \text{ cm}^{-1}$ , and  $1112 \text{ cm}^{-1}$  peaks were originated from carbonyl C=C, -OH, and C-O bonds in GO and SL, respectively [64–66]. The -OH bond peak disappeared at the GO/SL composite material after reacting with HDI and SL; this is due to GO reduction to rGO (Figure 8B). Zeta-potential for the rGO/SL composite was 75.14 mV. This indicates

that the significantly strong electrostatic repulsion force is formed against polysulfide ions, which is negatively charged, in order to suppress the LSB shuttling effect [67,68].

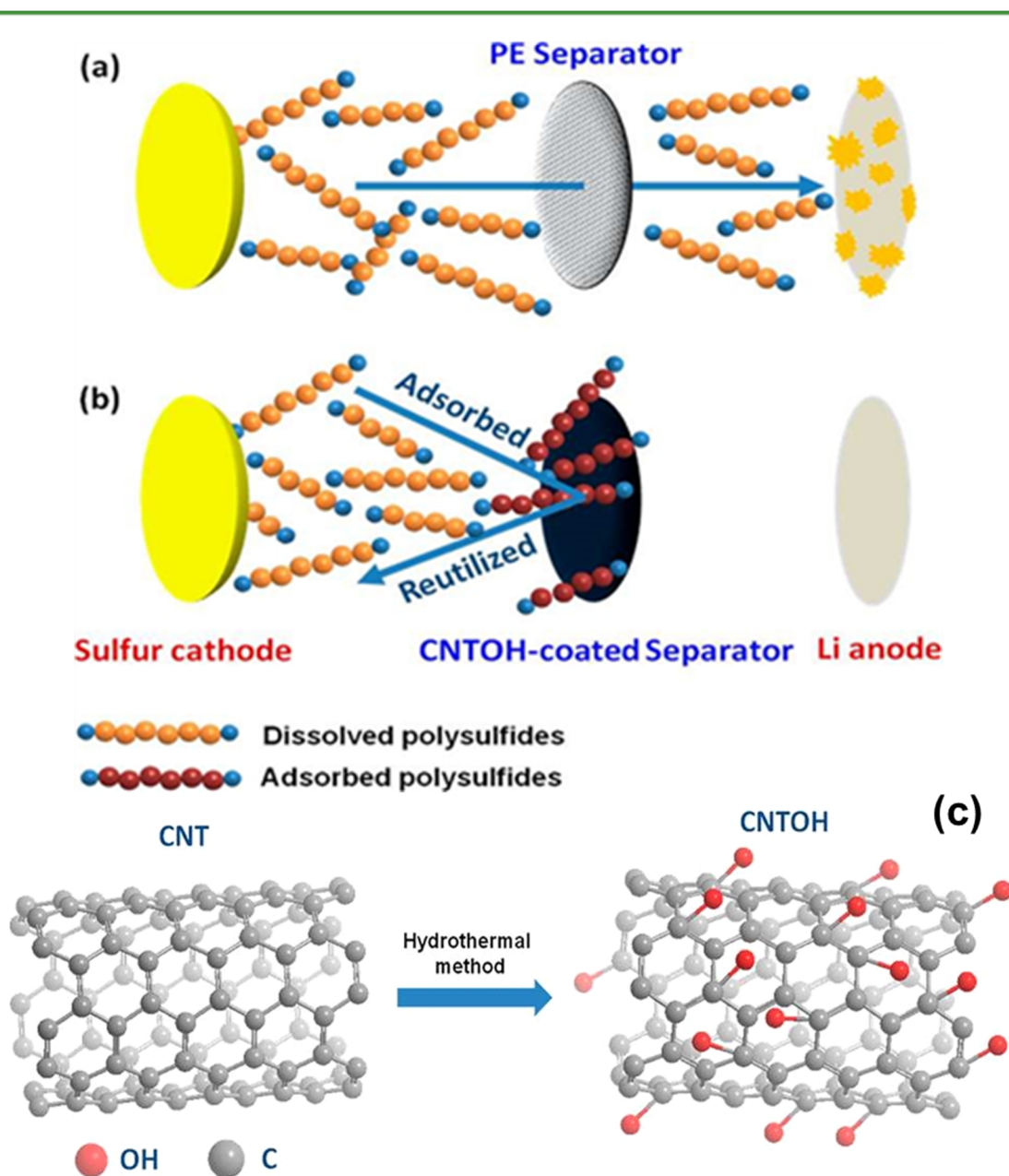


**Figure 7.** Speculated image of LiPS capture by the separator coated with CNTOH [63]. (a) LiPS transport to the anode side through separators, resulting in a decreased sulfur utilization. (b) In case of the separator with CNTOH application, hydroxyl functional groups on CNTOH would adsorb LiPS and utilized it to create polysulfides with short chains. (c) Surface treatment method of CNT via a hydrothermal procedure to form CNTOH.

This type of prepared rGO/SL composite solution was applied to a commercial PP separator using a facile vacuum filtration process. Sulfonic groups in the lignin can confer a separator with enough negative charge and reduce negatively charged LiPS diffusion. Applying this reduced graphene oxide/sodium ligno-sulfonate/separator achieved a capacity retention of 74% over 1000 cycles [69].

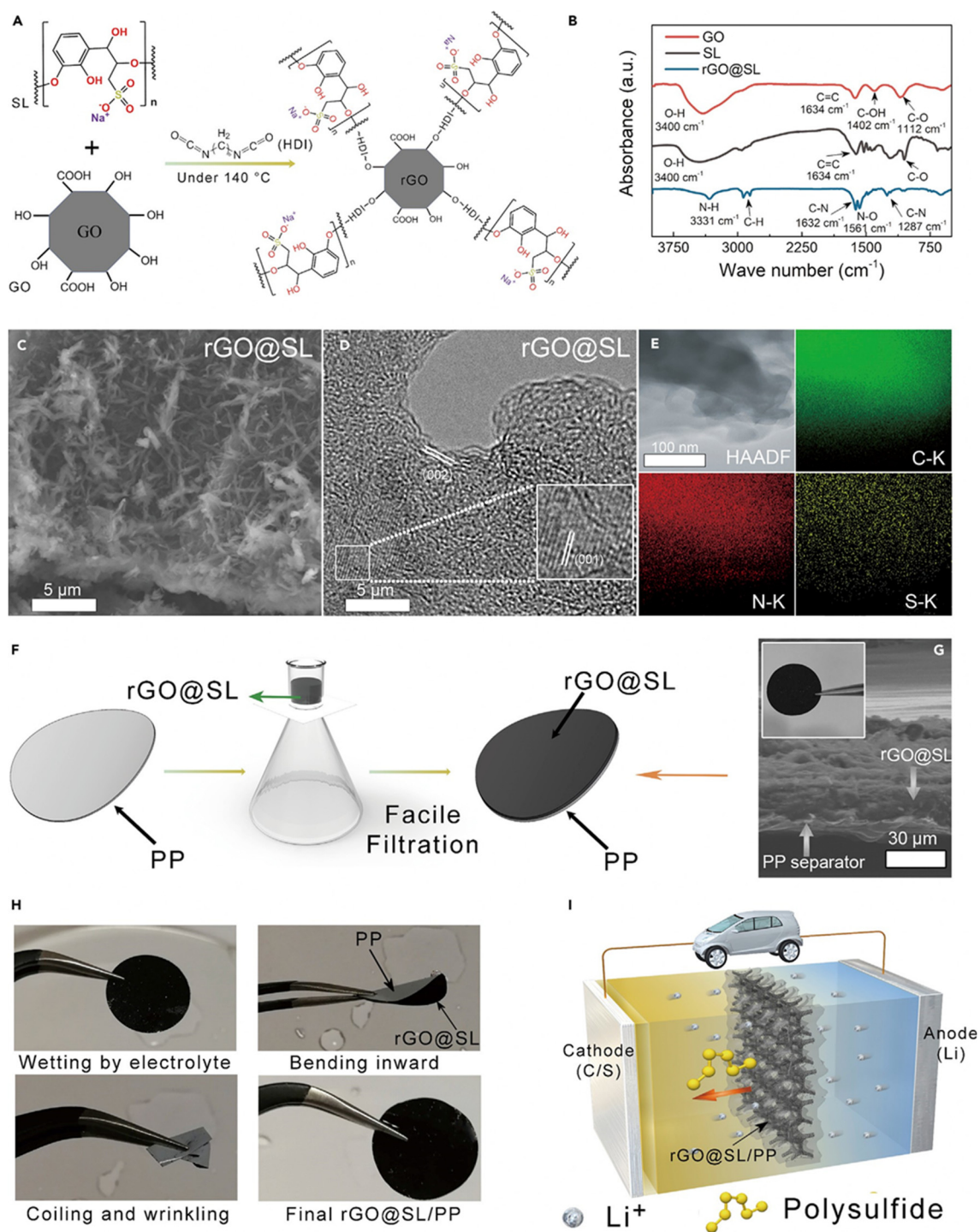


**Figure 8.** Synthesis procedure, microscopic observation and preparation of the rGO/SL composite and rGO/SL/PP separator [69]. (A) Preparation steps to make rGO/SL. (B) FTIR spectra of GO, SL, and rGO/SL. (C) Scanning electron microscopy images of the rGO/SL composite. (D) HRTEM observation of the rGO/SL composite. (E) Elemental analysis of C, N, and S for rGO/SL. (F) Preparation for the rGO/SL/PP separator. (G) Scanning electron microscopy picture of the rGO/SL/PP separator. (H) rGO/SL/PP separator image against mechanical stresses. (I) Speculated image of the rGO/SL/PP separators for suppressing LiPS shuttle effect.

In addition to simply physically blocking LiPS, chemical bonding between polar substances is an alternative procedure to suppress LiPS diffusion. To capture polar polysulfide, polar materials are superior to hydrophobic carbon materials. Carbonaceous materials

doped with various kinds of elements (e.g., N, B, S, P, F, O, Cl, Co, Ni, Fe) tend to possess polarity and have greater ability to capture LiPS [70]. The composite material composed of a nitrogen-doped reduced form of graphene oxide with  $\text{CoS}_2$  and  $\text{NiS}_2$  was made via a hydrothermal method [71]. Figure 9a shows the adsorption–desorption isotherms and pore size distribution of the cobalt nickel sulfur/nitrogen-doped reduced graphene oxide (CNS/N-rGO) composite and the one combined with sulfur, respectively. BET-specific surface area of CNS/N-rGO was  $177 \text{ m}^2/\text{g}$ , and the pore volume was  $0.416 \text{ cm}^3/\text{g}$ . The desorption isotherm of Barrett–Joyner–Halenda (BJH) is presented in Figure 9b. An obvious strong peak at 4 nm is proof of the porous structure of the sample, which can promote lithium ion transportation and help adsorb the LiPS, thus improving the LSB electrochemical performance [72,73]. However, after combining with sulfur, the pore volume and surface area significantly reduced, suggesting that the CNS/N-rGO was deeply immersed with sulfur. Figure 9c is the XRD pattern of the CNS/N-rGO composite material. A  $26^\circ$  broad peak can be ascribed to the (002) facet of the graphite. One can deduce that  $53.04^\circ$ ,  $49.03^\circ$ , and  $32.01^\circ$  peaks corresponded to the (200), (220), and (311)  $\text{CoS}_2$  facets, respectively [74]. Furthermore, characteristic peaks at  $1350 \text{ cm}^{-1}$  (D band) and  $1580 \text{ cm}^{-1}$  (G band) as can be observed in the Raman spectra are inferred to have derived from the structural defect and the stretching mode of the C–C bond of graphene, respectively [75]. Wu et al. coated this composite material onto a separator surface and used it in an LSB [71]. Owing to its morphological advantages and LiPS affinity, the LSB exhibited  $1524 \text{ mAh g}^{-1}$  at the first discharge and  $610 \text{ mAh g}^{-1}$  at 0.1 C and 8 C, respectively. It exhibited good long-term stability, with a  $700 \text{ mAh g}^{-1}$  capacity even after 350 cycles under 1 C. It was deduced that nitrogen doping and cobalt nickel, and sulfur nanoparticles in the composite, could provide a favorable electrochemical structure and active sites for capturing soluble LiPS and promote LiPS conversion in redox reactions, thus preventing the shuttle effect [74].

Some study. applied sulfur and metal, nitrogen co-doped carbon nanoparticles as the separator material for LSBs [76,77]. They were applied onto the separator to suppress LiPS diffusion. It was found that for nitrogen, the sulfur co-doped carbon nanoparticles improved both capacity and cycle characteristics. The capacity was  $841 \text{ mAh g}^{-1}$  at 0.2 C even after 100 cycles with a 99.3% of coulombic efficiency.

Song et al. used a lightweight, functional layer composed of porous iron and nitrogen-co-doped carbon nanofiber materials to modify a PP separator for LSB. The Fe–N-co-doped carbon possesses high conductivity and LiPS adsorption capability to the separator, which was effective in preventing LiPS diffusion. Prepared separator behaved as the conductive current collector to reuse the active sulfur-based compounds as well.

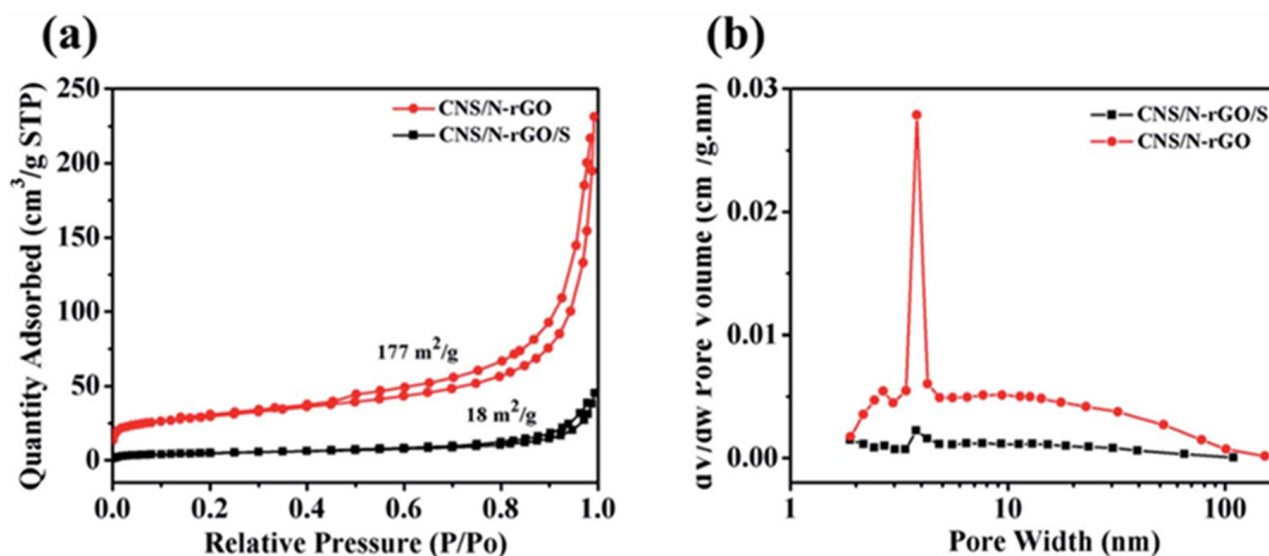
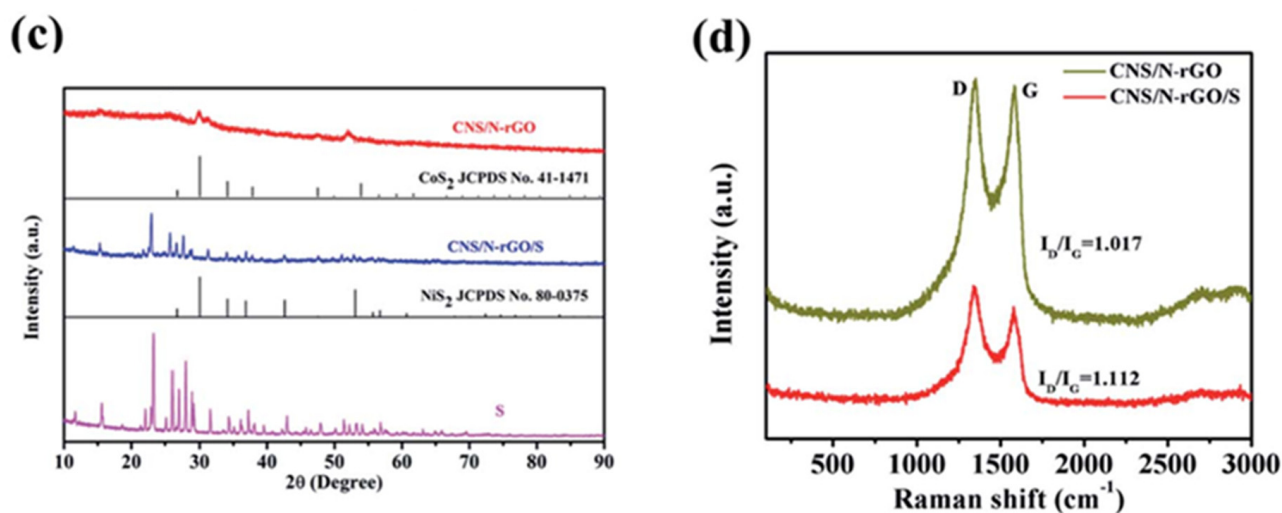


Figure 9. Cont.



**Figure 9.** (a) The adsorption–desorption isotherms of N<sub>2</sub>. (b) BJH pore size distribution curves of the CNS/N-rGO composite and CNS/N-rGO/S. (c) XRD pattern of the CNS/N-rGO composite. (d) Raman spectrum of the CNS/N-rGO composite [72].

### 2.2.2. Separator Material: Metal Oxide

Metal oxides were investigated for application as LSB separators as they can generate different bonds for LiPS. Metals lose their electrons in certain conditions and become metal ions, which can generate chemical bonds to capture LiPS to prevent the shuttle effect. In addition, the metal oxides in nanostructure states would be easier to combine with polymers to become functional separators. It has been shown that LiPS diffusion can be suppressed with the Al<sub>2</sub>O<sub>3</sub>-coated layer on the separator's cathode side as a physical block layer for LiPS. The first discharge capacity of the LSB prepared with an Al<sub>2</sub>O<sub>3</sub>-applied separator was 967 mAh g<sup>-1</sup> at 0.2 C and deteriorated to 593.4 mAh g<sup>-1</sup> after 50 cycles. The electrode resistance was reduced because of the porous structure of the Al<sub>2</sub>O<sub>3</sub>-coated layer that worked as an ion-conducting scaffold for capturing sulfur containing active materials [78].

Han et al. created a PP separator with a TiO<sub>2</sub>/carbon-coated layer and applied it to an LiPS capturing barrier for LSB [76]. The highly conductive carbon with its porous structure endowed the separator with the ability to adsorb LiPS while acting as a second electrical current collector. In addition, TiO<sub>2</sub> on the porous carbon surface captured LiPS. Owing to these properties of the TiO<sub>2</sub>/porous carbon composite material, 926 mAh g<sup>-1</sup> capacity was observed initially at 0.1 C; also, it maintained a 75% capacity even after 150 cycles [79].

Gao et al. also prepared a separator coated with a TiO<sub>2</sub>/surface-modified carbon nanotube composite. The LSB assembled with this type of separator—having strongly polar TiO<sub>2</sub> and highly conductive carbon nanotubes—demonstrated an enhanced battery performance. The capacity was initially 1104 mAh g<sup>-1</sup> and was still as high as 848 mAh g<sup>-1</sup> even after 200 cycles at 0.5 C, demonstrating a capacity decay of only 0.066% per cycle over 900 cycles [80].

A SiO<sub>2</sub> nanoparticle-modified PP separator was made by Li et al. by dipping a PP separator into a sol–gel TEOS solution and Tween-80 [78]. This kind of separator has high wettability and thermal stability, and the resulting LSB showed considerable improvement in its electrochemical performance. The capacity decay of the LSB prepared with this SiO<sub>2</sub>–PP separator was 64% after 200 cycles at 0.2 C, which was superior than the one made with a commercial separator (45%). In addition, the capacity of LSB with SiO<sub>2</sub>–PP separator achieved 956.3, 691.5, 621, and 567.6 mAh g<sup>-1</sup> at a 0.2, 0.5, 1, and 2 C current density, respectively [81].

Increasing the ratio of sulfur utilization would increase LSB capacity. Thus, it is necessary to not only capture LiPS, but also to reactivate sulfur [82]. Certain types of separators with adsorption abilities cannot satisfy this requirement. Therefore, it is necessary to look

for the material which can play a role for LiPS reutilization. In addition, the material with catalytic ability is also important.

During the LSB charging process, fast-reaction kinetics is achieved only when the energy which is higher than the activation energy of solid  $\text{Li}_2\text{S}_2/\text{Li}_2\text{S}$  conversion to polysulfide is applied [83]. Fast battery reaction rate can be accelerated when activation energy is lowered so that one needs a good catalyst to lower the activation energy. This concept differs from the LiPS adsorption materials, which we have previously described above. This kind of catalytic material can accelerate the oxidation reduction rate so that the reaction of polysulfides' conversion reaction to  $\text{Li}_2\text{S}_2/\text{Li}_2\text{S}$  can be enhanced. This is also a highly efficient way to prevent the LiPS shuttle problem besides using LiPS adsorption materials. Electrons on the catalytic material can transport to the S-S bond of LiPS to become  $\text{Li}_2\text{S}_2/\text{Li}_2\text{S}$ . In addition, the catalyst can reduce the overpotential of the sulfur species, which would enhance the sulfur electrochemical reactions [84]. Therefore, finding the appropriate catalytic material that can accelerate LiPS conversion into  $\text{Li}_2\text{S}_2/\text{Li}_2\text{S}$  is highly recommended.

In this regard,  $\text{La}_2\text{O}_3$  was coated onto a commercial PP separator in order to adsorb LiPS and accelerate redox reactions at the same time [85]. Charge/discharge measurements demonstrated that the resulting LSB showed a  $966 \text{ mAh g}^{-1}$  capacity on the first cycle at 1 C and the capacity became  $720 \text{ mAh g}^{-1}$  after 200 cycles. It was suggested that the enhanced electrochemical properties were due to the LiPS capturing effect of  $\text{La}_2\text{O}_3$  as well as being a chemical catalyst to promote the electrochemical reaction by lowering the activation energy [85].

### 2.2.3. Separator Material: Metal Sulfide

Some metal sulfides are known to adsorb LiPS, owing to their polar nature, and thus have been studied for use as a separator material. Tan et al. prepared a reduced graphene oxide/ $\text{MoS}_2$  (rGO/ $\text{MoS}_2$ ) layer on the cathode side of the commercial separator. The rGO behaves as a barrier for LiPS diffusion and an extra current collector, while  $\text{MoS}_2$  can capture LiPS. The prepared LSB demonstrated  $1122 \text{ mAh g}^{-1}$  at 0.2 C, with a low capacity fading rate of 0.116% for 500 cycles at 1 C, and an excellent performance rate of  $615 \text{ mAh g}^{-1}$  at 2 C [86].

Another study demonstrated the potential use of edge-rich  $\text{MoS}_2/\text{C}$  hollow microspheres as LSB separators. The  $\text{MoS}_2/\text{C}$  hollow microspheres were prepared via hydrothermal synthesis with  $\text{MoO}_3$ , aniline, thiourea, and sucrose, following a carbonization process [87]. Carbonization was carried out in order to improve the graphitization degree of the carbon in  $\text{MoS}_2/\text{C}$  hollow microspheres (Figure 10). The prepared  $\text{MoS}_2/\text{C}$  hollow microspheres carry a high chemical absorption property and a high density of LiPS-capturing sites, resulting in showing excellent LiPS diffusion prevention. In addition, the phase conversion reversibility of the active sulfur species could be regulated in a stable manner with this  $\text{MoS}_2/\text{C}$  composite material particularly at high C-rates and sulfur loading. Thus, the LSB arranged with the  $\text{MoS}_2/\text{C}$  separator exhibited a capacity of  $935 \text{ mAh g}^{-1}$  at an initial cycle at 1.0 C and it was  $494 \text{ mAh g}^{-1}$  even after 1000 cycles [88].

Functional separators using two-dimensional exfoliation nanosheets could efficiently contain LiPS for long-life LSBs. Mao et al. fabricated new two-dimensional ZnS exfoliation nanosheets using the microwave-assist exfoliation method, and then combined it with graphene to modify a commercial separator. The nanosheet dispersion was mixed with graphene and filtered on the separator to form ZnS exfoliation nanosheets/graphite/Celgard separators. An LSB assembled with this type of separator exhibited an  $1165.9 \text{ mAh g}^{-1}$  as initial capacity and became  $685.3 \text{ mAh g}^{-1}$  after 100 cycles. Capacity was 58.8% compared to the initial one at 0.1 C and 0.036% of capacity decay per cycle when the cycle was carried out for 1000 times at 0.5 C [89].

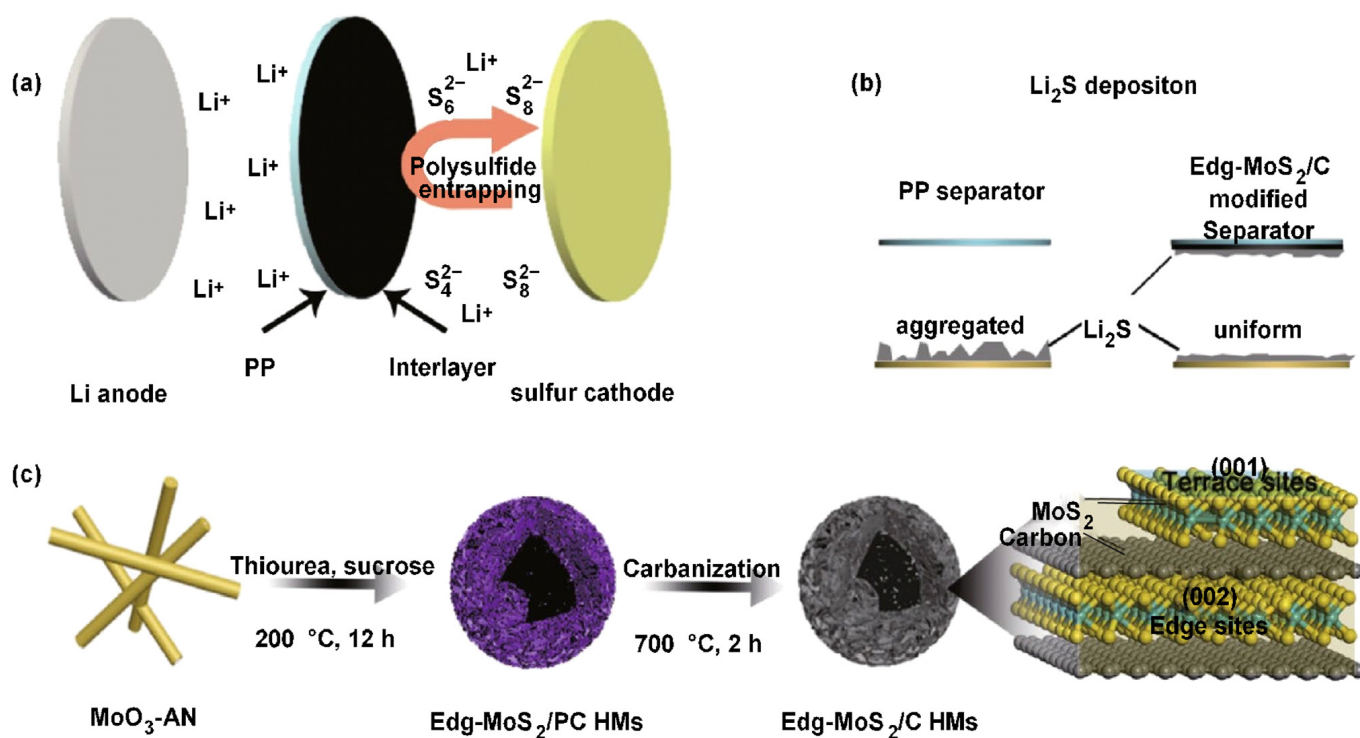


**Figure 10.** Schematic model of the operation and preparation of the Edge-MoS<sub>2</sub>/C/PP separators [87]. (a) Image illustration of polysulfides' capture in LSB with Edge-MoS<sub>2</sub>/C/PP separator. (b) Image illustration of Li<sub>2</sub>S deposition on the separator with edge-MoS<sub>2</sub>/C/PP and PP. (c) Synthesis procedure of the Edge-MoS<sub>2</sub>/C hollow microspheres and illustration of the Edg-MoS<sub>2</sub>/C hollow microspheres.

Yao et al. utilized the high conductivity and absorption ability of SnS, and the strong catalytic property of ZnS, to prepare a ZnS–SnS heterojunction [84]. A polydopamine-derived nitrogen-doped carbon was coated onto this ZnS–SnS composite material and was compared with its single-component counterparts (ZnS/N-doped carbon shell and a SnS/N-doped carbon shell). When coated onto the separator, the ZnS–SnS/N-doped carbon-based LSB demonstrated a high reversibility of 1149 mAh g<sup>-1</sup> capacity for 300 cycles at 0.2 C, and a 661 mAh g<sup>-1</sup> at 10 C, and capacity decay was 0.0126% each cycle after 2000 cycles at 4 C [90].

In addition, it was reported that a WS<sub>2</sub>/Prussian blue (PB)–PPy composite material-modified separator could inhibit the back and forth movement of LiPS and the formation of inactive sulfur-related substances. Lithium ions, however, could still be transferred homogeneously inside the battery. When compared with the LSB with ordinary commercial PP separators, the capacity and cycle properties of this modified LSB were remarkably ameliorated and showed high capacity (1050 mAh g<sup>-1</sup>) and improved capacity retention (650 mAh g<sup>-1</sup> after 300 cycles) as well as a capacity retention rate that reached 62%. This study also showed that three porous layers as an ion-sieve structure indeed prevents the transfer of LiPS through the electrolyte to the anode [91].

#### 2.2.4. Separator Material: Metal Carbide

Titanium carbide (TiC) is regarded as a representative non-oxide ceramic material with high electrical and thermal conductivity, robust hardness, and high chemical stability [92]. In a recent study, TiC is acknowledged to be utilized for energy storage purposes owing to these excellent properties. Especially for LSBs, TiCs are considered to improve the cycle stability via its high polarity to capture sulfur species and its ability to reduce the LiPS shuttle effect [93]. In addition, the high electrical conductivity of TiC is an additional good reason for it to be an ideal sulfur scaffold material.

Liu et al. synthesized TiC nanoparticles from waste polytetrafluoroethylene as a carbon source at 500 °C, that is lower than general TiC synthesis temperature. They used this TiC as a coating material for an LSB separator and successfully mitigated the shuttling problem. The visual influence was investigated by dispersing prepared TiC nanoparticles in an LiPS solution. At the TiC–Li<sub>2</sub>S<sub>6</sub> bottle, the yellowish color became more transparent after two hours of adsorption, whereas the bottle without TiC remained unchanged, as presented in Figure 11A,B. These results clearly imply that waste polytetrafluoroethylene-derived TiC nanoparticles have high potential in reducing LiPS shuttle effect in LSBs [94]. The bending exam proved TiC's strong adhesion to the separator as shown in Figure 11C. One can easily visualize that the dissolved LiPS shuttle effect could be suppressed with this separator. A capacity as high as 1242 mAh g<sup>-1</sup> was detected at the first cycle with the LSB prepared with the TiC-attached separator, and even after 100 cycles, a 736 mAh g<sup>-1</sup> capacity was retained, which are superior results compared to an LSB with a commercial separator (respectively, 827 and 373 mAh g<sup>-1</sup>). They also proved that the high electronic conductivity of the TiC resulted in a low capacity decay during rate performance [95]. Zhao et al. also fabricated a novel TiC-modified PP separator and applied it as an LBS separator. Compared to the commercial separator, the TiC-modified separator exhibited superior wettability and adsorption ability for LiPS. As a result, the LSB with a TiC-modified PP separator displayed a higher specific capacity and more stable cycling performance [96].

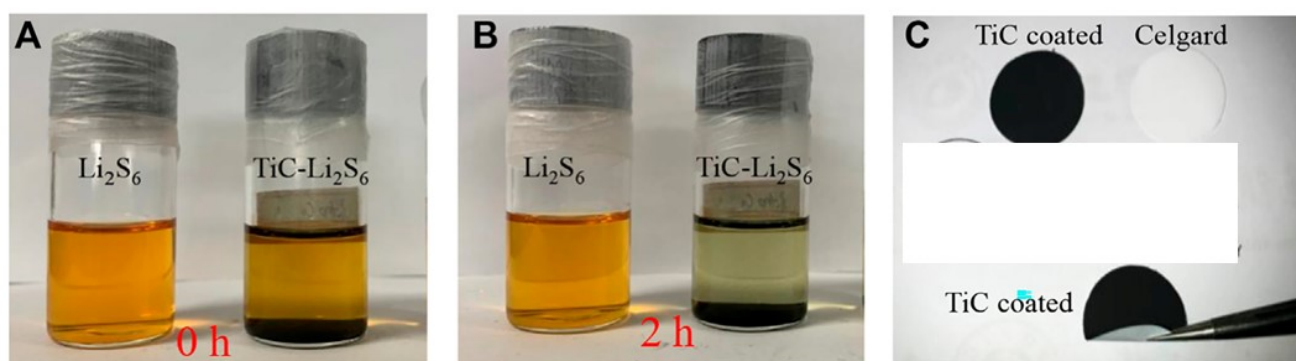


**Figure 11.** The pictures of LiPS capturing: (A) Before and (B) after 2 h. (C) Digital image of the TiC-coated separator and bent testing image [94].

Moon et al. made an LSB assembled with a separator that contained mesoporous tungsten carbide (meso-WC) and reduced graphene oxide [91]. The battery exhibited good performance: ~950 mAh g<sup>-1</sup> at 1 C after 100 cycles. It was deduced that the improved characteristics were due to the shuttle effect reduction due to the high adsorption of LiPS, the effective reutilization of active materials, and the acceleration of the conversion reaction [97].

A Co<sub>3</sub>W<sub>3</sub>C/C composite was prepared by Zhao et al. [94] using a simple pyrolysis procedure, and it was applied on a commercial separator. The Co<sub>3</sub>W<sub>3</sub>C/C-modified separator was effective in reducing the shuttle effect. In addition, it worked as a catalytic membrane to promote the redox reaction of the sulfur species. For the LSB prepared with the Co<sub>3</sub>W<sub>3</sub>C/C-coated separator, 1345 mAh g<sup>-1</sup> at 0.1 A g<sup>-1</sup> was observed as initial discharge capacity. Rate performance was also good by achieving high capacity of 670 mAh g<sup>-1</sup> even at 7 A g<sup>-1</sup>. Cycle performance was also excellent since the decay rate was as low as 0.06% per cycle within 500 cycles at 1 A g<sup>-1</sup>. These results indicate that this material utilizes Co–W metallic carbide advantage in capturing LiPS and promote the electrochemical reaction to gain high-performance LSB [98].

A nanocrystalline niobium carbide was synthesized using practical scalable autoclave technology and was used as the interlayer material for an LSB by Cai et al. [95]. The prepared nanocrystalline niobium carbide exhibited a strong ability to anchor LiPS species,

which were highly effective in improving cycling performance and rate capabilities. The conductive niobium carbide interlayer not only acted as a shield to confine LiPS within the cathodic side, but also acted as the second current collector to reutilize the trapped active material and significantly enhance sulfur utilization. Because of these superior characteristics, the LSB assembled with this type of separator showed outstanding cycle stability and electrochemical performance<sup>-2</sup> [99].

#### 2.2.5. Separator Material: Nitride

Transition metal nitrides have been applied as a catalyst and as electroanalysis devices because of their high conductivity, reactivity, and stability [100]. For example, in contrast to their oxide ( $1.0 \times 10^{-3} \text{ Sm}^{-1}$ ) and sulfide ( $9.7 \times 10^{-2} - 10^3 \text{ Sm}^{-1}$ ) counterparts, molybdenum nitrides possess high electrical conductivity [101]. Chen et al. applied molybdenum nitride on a commercial separator and the capacity of the assembled LSB was  $566 \text{ mAh g}^{-1}$  after 500 cycles at 0.5 C [102].

Kim et al. prepared a boron nitride nanotube (BNNT)-based separator for the cathode side. Lithium stripping/plating analysis was conducted to elucidate the lithium metal's stability by observing the overpotential. When stripping/plating of lithium was conducted at  $0.35 \text{ mA/cm}^2$ , a similar overpotential profile was observed for LSBs composed of all separator types; however, when it was carried out at  $1 \text{ mA/cm}^2$ , the overpotentials of the commercial and BNNT separator were much more obvious than those of the p-BNNT (Figure 12a,b). This occurred because of dendrite formation and detachment caused by non-uniform lithium stripping/plating. In contrast, the higher ionic conductivity of the p-BNNT separator demonstrated the good stability of the lithium anode (Figure 12c-e). The p-BNNT also showed a uniform pore structure due to partial charge on the surface, which is a result of the electronegativity difference between B and N. Thus, in contrast to the commercial separator, the p-BNNT-applied separator suppresses dendrite growth on the Li metal anode, promotes ion transfer, and mitigates LiPS diffusion. Owing to these characteristics, the capacity of the p-BNNT-loaded PP separators-based LSB was  $1429 \text{ mAh/g}$  and exhibited stability until 200 cycles [103].

Chen et al. also prepared high-quality boron nitride nanosheets using a scalable exfoliation process and used them as a separator material [101]. They implemented the sonication-assisted liquid-phase exfoliation scalable process and investigated the effects of a spectrum of exfoliation factors (e.g., ultrasonic conditions and solvent and bulk material feeding) on the boron nitride nanosheet yield. A high yield of 72.5% could be achieved while maintaining the boron nitride nanosheets to a few layers and is defect free. Owing to the Lewis acid sites of the boron atoms, the boron nitride nanosheets could interact with the polysulfide anions in the liquid electrolyte and facilitate uniform lithium deposition, with the end result being an LSB with a long life [104].

Carbon nitride was used as an LSB separator material by Luo et al. [99]. Co-doped g-C<sub>3</sub>N<sub>4</sub> nanosheets were synthesized via a calcination process. The capacity of the LSB prepared with the Co-g-C<sub>3</sub>N<sub>4</sub>-modified separator was  $1121 \text{ mAh g}^{-1}$  at 0.2 C with a high performance rate of up to 3 C. The Co-g-C<sub>3</sub>N<sub>4</sub>-modified separator-installed LSB also indicated an excellent stability of  $640 \text{ mAh g}^{-1}$  after 250 cycles. This amelioration was because of the restriction of LiPS diffusion owing to the high adsorption and high efficiency of LiPS catalytic conversion induced by the Co-g-C<sub>3</sub>N<sub>4</sub> nanosheet-implemented separator [105].

#### 2.2.6. Separator Material: Phosphide

Transition metal phosphides generally have good electrical performance, adequate chemical adsorption ability, and significantly high catalytic capability for LiPS, which makes them an interesting choice as a separator modifier for LSBs [106].

Chen et al. applied CoP nanospheres as a separator coating material for LSBs [101]. It was found that the conductive CoP could efficiently anchor LiPS because of its polar nature and partial surface oxidation state (as confirmed via the XPS analysis), which induce Co

sites to chemically capture LiPS with Co–S bonding. Owing to these characteristics, this LSB exhibited high electrochemical characteristics and excellent rate performance ( $725 \text{ mAh g}^{-1}$  at 5 C) [107].

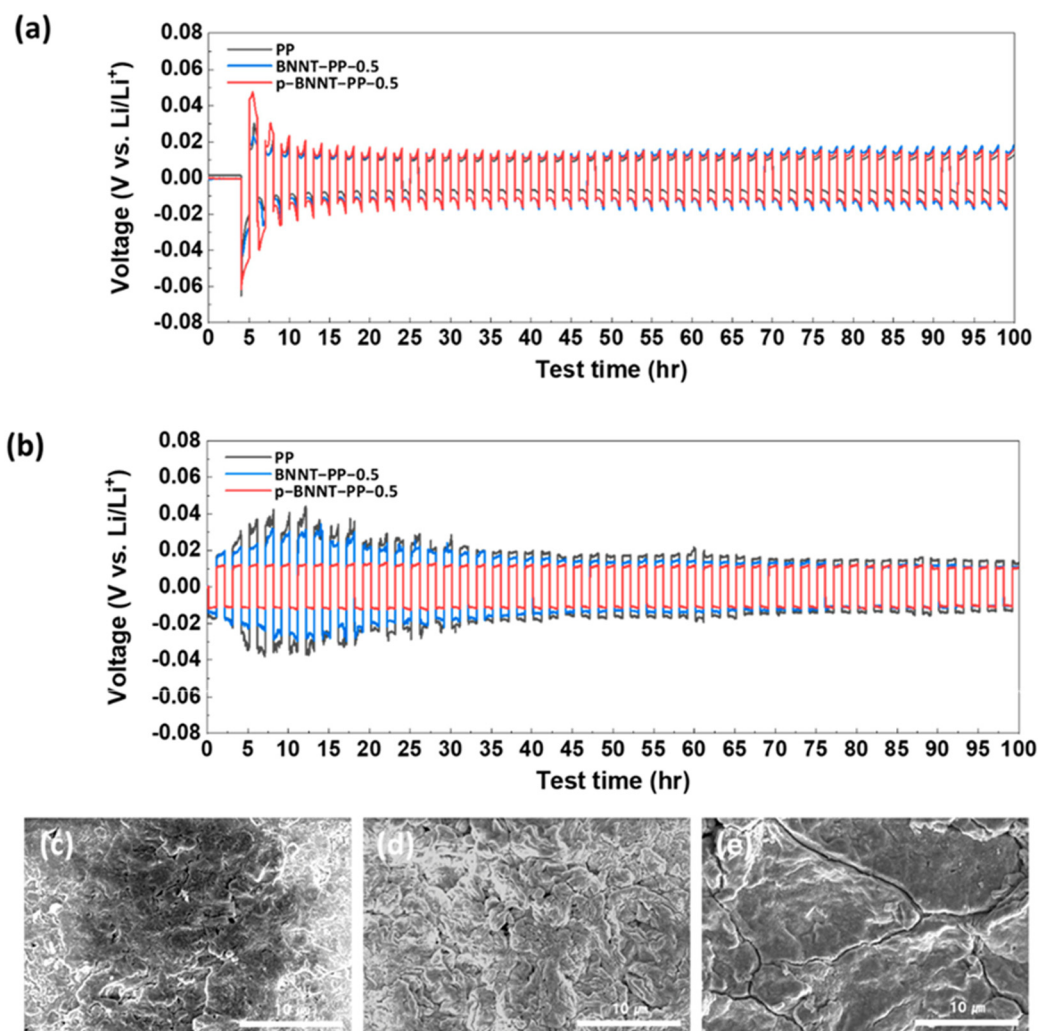


**Figure 12.** Lithium stripping/plating reaction with PP, BNNT, and p-BNNT-applied separator at (a)  $0.35 \text{ mA/cm}^2$  and (b)  $1 \text{ mA/cm}^2$ . Top view of SEM observation of lithium metal after lithium stripping/plating reaction with (c) PPY (d) BNNT-PP-0.5, and (e) p-BNNT-PP-0.5 [103].

Lin et al. also investigated the possibility of CoP as a separator coating material [106]. They modified a PP membrane with nano-cubic CoP/C. CoP/C-deposited separator captured LiPS with high efficiency via its strong chemical affinity. The LSB arranged with the CoP/C-deposited separator presented a minimum capacity decay as low as 0.08% per cycle over 500 cycles at 1 C with a  $938 \text{ mAh g}^{-1}$  capacity as the initial cycle. Rate performance was  $594 \text{ mAh g}^{-1}$  at 4 C [108].

Another transitional metal phosphide was also studied by Zhao et al., who prepared FeP/spongy carbon composites with multiple adsorptions and catalytic sites as a modified material for an LSB separator [109]. The spongy carbon was shown to possess suitable structural stability and long ion/electron transmission channels. The addition of the FeP-endowed spongy carbon reacted with the LiPS to block shuttling and catalyze the conversion of sulfur. It was found that the FeP/spongy carbon-modified separator could reduce the flammability of the completed LSB. Benefiting from these features, the prepared LSB exhibited high cycling stability and the LSB could retain a  $618 \text{ mAh g}^{-1}$  capacity even after 150 cycles [109].

A heterostructured Ni/Ni<sub>2</sub>P-embedded mesoporous carbon nanosphere composite (Ni/Ni<sub>2</sub>P-MCN) was developed to accelerate polysulfide catalytic conversion in LSBs.

Figure 13 indicates cyclic voltammetry curves of an LSB prepared with four types of separators. Two cathodic peaks can be ascribed to the sulfur transition of soluble polysulfides to solid-state Li<sub>2</sub>S<sub>2</sub>/Li<sub>2</sub>S, and they are stronger for the LSB prepared with Ni/Ni<sub>2</sub>P-MCN. Thus, it can be suggested that Ni/Ni<sub>2</sub>P-MCN can enhance the efficiency of polysulfide conversion kinetics [110]. One can also observe the anodic peak approximately at 2.4 V. The one with Ni/Ni<sub>2</sub>P-MCN/PP indicated an anodic peak with a lower potential than the remaining three types, proving an enhanced Li<sub>2</sub>S<sub>2</sub>/Li<sub>2</sub>S oxidation reaction [111,112].

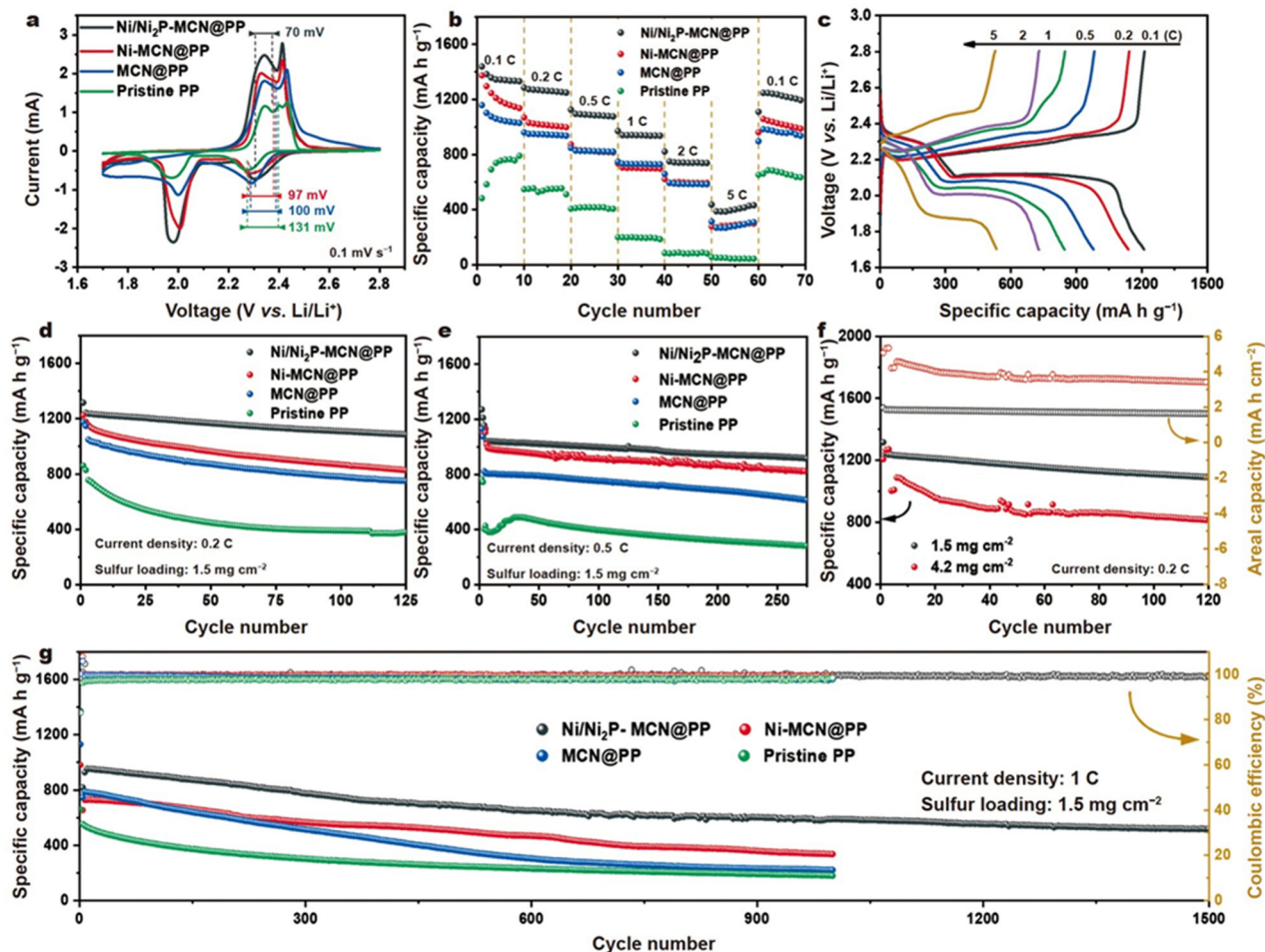


**Figure 13.** (a) Cyclic voltammetry. (b) Rate performances of LSB prepared with Ni/Ni<sub>2</sub>P-MCN/PP, Ni-MCN/PP, MCN/PP, and commercial PP. (c) Charge–discharge profiles of LSB prepared with Ni/Ni<sub>2</sub>P-MCN/PP at various current densities from 0.1 to 5 C. (d,e) LSB cyclic performance prepared with Ni/Ni<sub>2</sub>P-MCN/PP, MCN/PP, and pristine PP at 0.2 and 0.5 C. (f) LSB cycling performance prepared with Ni/Ni<sub>2</sub>P-MCN/PP at 0.2 C. (g) LSB cycling performance prepared with Ni/Ni<sub>2</sub>P-MCN/PP, MCN/PP, and commercial PP at 1 C [110].

The Ni/Ni<sub>2</sub>P-MCN/PP LSB also presented the strongest capacity among all LSBs (Figure 13b). Figure 13c presents the charge–discharge curves and the Ni/Ni<sub>2</sub>P-MCN/PP LSB showed a weak degree of polarization, a typical discharge plateau, indicating its relatively high sulfur utilization. As shown in Figure 13d, the Ni/Ni<sub>2</sub>P-MCN/PP LSB delivered an initial discharge capacity of 1315 mAh g<sup>−1</sup> at 0.2 C and retained a capacity of 1086 mAh g<sup>−1</sup> after 125 cycles. When the applied current was increased to 0.5 C (Figure 13e), the discharge capacity was still 916 mAh g<sup>−1</sup> and a high capacity retention was maintained to keep approximately 87.9% even after 275 cycles.

The Ni/Ni<sub>2</sub>P–MCN/PP LSB indicated an enhanced discharge capacity of 815 mAh g<sup>-1</sup> even after 120 cycles (Figure 13f). An extended cycling performance test was conducted and the Ni/Ni<sub>2</sub>P–MCN/PP LSB presented a discharge capacity of approximately 953 mAh g<sup>-1</sup> at 1 C (Figure 13g). It had an excellent discharge capacity of approximately 518 mAh g<sup>-1</sup> even after 1500 cycles. Thus, we can say that the Ni/Ni<sub>2</sub>P-mesoporous carbon nanosphere composite-deposited separator not only suppressed the LiPS diffusion by their chemical capturing sites, but also possesses strong catalytic abilities for the polysulfide reactions.

#### 2.2.7. Separator Material: Metal Organic Framework-Based Materials

Metal organic frameworks (MOFs) are the class of porous materials composed of metal ions and organic ligands. One of MOF application can be molecular sieves and selective gas separation on a molecular scale [113–117]. MOF and MOF-based composite materials have been investigated as porous host materials for LSB cathodes to retain sulfur due to their large specific surface area and catalytic effect for LiPS. A porous material with optimally regulated pore sizes can work as a sieve to separate desirable ions from an ionic solution such as LiPS, thus resulting in reducing their shuttle effect. In this regard, MOF and MOF-based materials are good candidate materials for LSB separators owing to their tunable pore size and specific surface area.

Songyan et al. prepared an MOF-based LSB separator to investigate its effectiveness in mitigating the LiPS shuttling issue [118]. The separator behaved as an ionic sieve for LSB and successfully sieved Li<sup>+</sup> ions while mitigating LiPS migration to lithium metal anode side.

One example is in applying MOF–graphene oxide composite as a separator material. The preparation procedure is exhibited in Figure 14a. The MOF layer was grown initially. A desirable amount of graphene oxide (GO) solution, which was obtained by filtration, was applied onto uniformly dispersed crystalline MOF particles. It was confirmed that the MOF and GO layers were strongly adhered onto the membrane. This procedure was repeated several times to assure the quality of the preparation process. The MOF nanoparticles filled the void space tightly near the grain boundaries. A self-standing separator can be obtained by peeling off this type of material from the filter. It was found that the structural scaffold of the MOF remained intact even after over 200 electrochemical cycles. (Figure 14c). The morphological observation of the MOF/GO separator is presented in the SEM image (Figure 14d,e). When this type of MOF-based separator was implemented as a separator, the resulting LSB exhibited a low decay rate, as low as 0.019% per cycle in a long duration of up to 1500 cycles. Almost no capacity fade was observed at the initial 100 cycles [118].

Dang et al. prepared a composite membrane separator composed of cerium-based UiO-67 (MOF) and a glass fiber. The prepared Ce-UiO-67 efficiently adsorbed LiPS and catalyzed its conversion, thus suppressing the associated shuttle effects. In addition, this type of MOF theoretically provides rich lithiophilic functional groups to attain rapid Li<sup>+</sup> ion transportation, leading to achieving stable Li plating and stripping. The resulting LSB delivered 919 mAh g<sup>-1</sup> at initial cycle and a small decay rate of 0.04% per cycle for 500 cycles at 1 C [119].

Su et al. also prepared a cerium-based MOF separator and used Ce-UiO-66-NH<sub>2</sub> as the MOF material. Strong interaction between LiPS and the metal sites in UiO-66-NH<sub>2</sub>, as well as being the physical barrier for LiPS, enabled this type of separator to inhibit the shuttle effect. The assembled LSB offered a high capacity of 1366 mAh g<sup>-1</sup> initially with a stable cycling property at 0.2 C. In addition, capacity decay was only 0.09% per cycle at 300 cycles at 1 C [120].

A conductive carbon (Ketjenblack) and zeolite imidazole framework-8 (ZIF-8)/polypropylene composite separator was prepared by Ma et al. [115]. ZIF-8 and Ketjenblack were mixed in a 1:4 mass ratio in ethanol for 24 h, and then ultrasonically dispersed for 20 min. After that, the homogeneous solution was coated onto a commercial separator via vacuum filtration and was followed by vacuum drying at 60 °C for 24 h. The resulting separator comprised Ketjenblack, ZIF-8, and PP with a low coating load of 0.06 mg cm<sup>-2</sup>.

Ketjenblack/ZIF-8/PP can efficiently absorb LiPS due to a Lewis acid–base interaction between ZIF-8 and LiPS. This interaction could decrease the dissolution of LiPS as well as the shuttle effect, thereby enhancing the electrochemical properties of the assembled LSB. When 0.1 C of current density was applied, the assembled LSB exhibited low polarization, a capacity of 1235.6 mAh/g initially, and good capacity retention rate of 59.27% after 100 cycles [121].

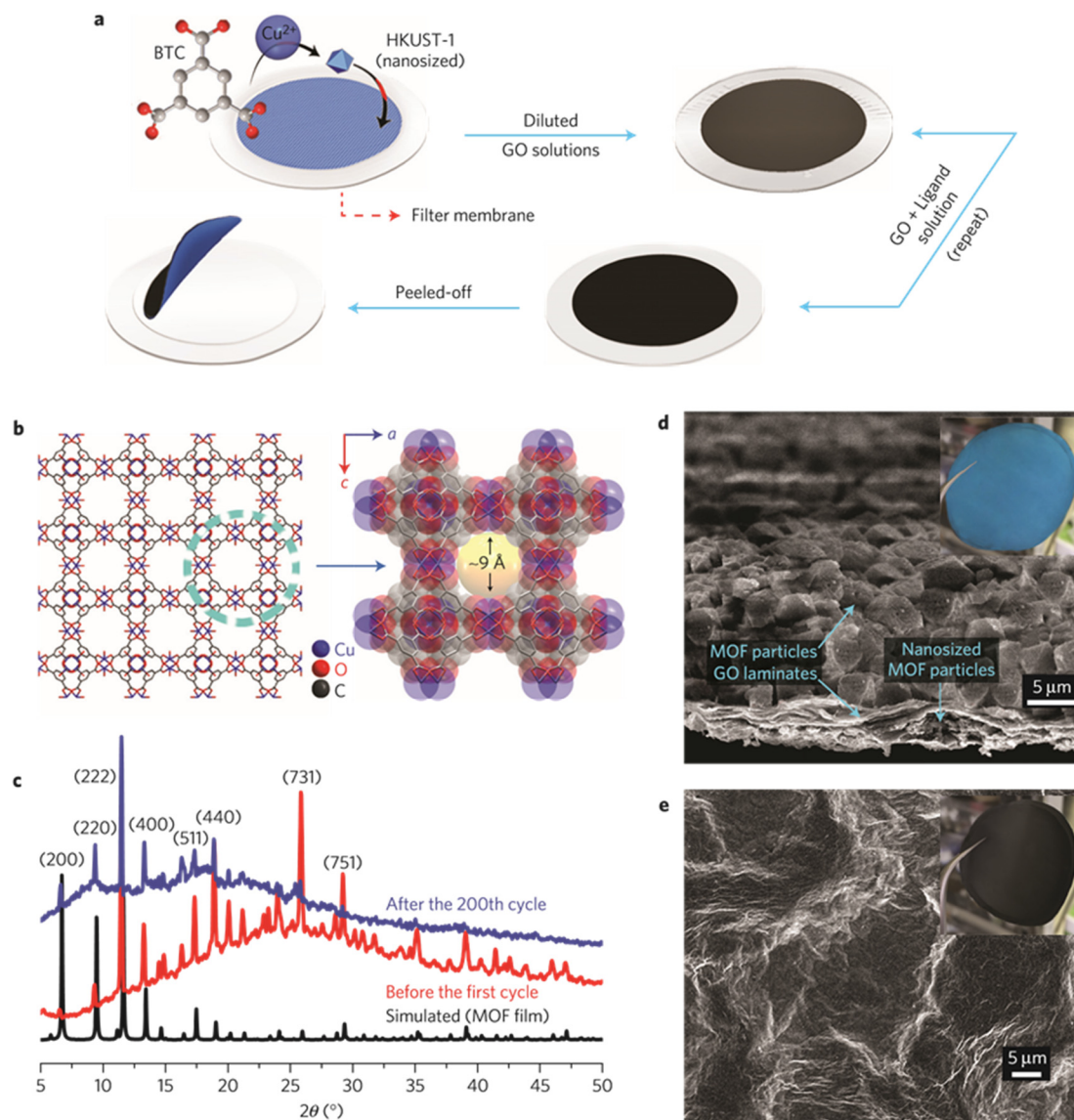


**Figure 14.** Preparation and material characteristics of MOF/GO separators [118]. (a) Illustration of preparation method to make MOF/GO separators. (b) Schematic image of HKUST-1. (c) PXRD patterns of MOF/GO separators. MOF structure remains unbroken after the discharge/charge process. (d) SEM photographs of the MOF/GO separator. The inset presents a digital image from the MOF side aspect. (e) SEM photograph of GO layer. The inset is an image from the GO side aspect.

### 2.2.8. Separator Material: Quantum Dot

Quantum dots (QDs) are generally super small crystalline particles with a size range of 1.0–10 nm. Recently, QDs have gained much attention for being interesting materials for electrochemical energy storage due to their large specific surface area, tunable size, short ion/electron transportation path, adjustable photoluminescence, and feasible surface functionalization [122,123]. In addition, it was reported that QDs can modify separators to suppress the shuttle effect, owing to their effective interaction with LiPS [124].

Atomic-layer deposition method was applied to prepare a TiO<sub>2</sub> quantum dot-modified multiwalled carbon nanotube as the deposition material for LSB separators and succeeded in preventing the LiPS shuttling effect and improving the coulomb efficiency and cycle stability (Figure 15a) [121]. It was suggested that these positive effects were achieved due to an interaction between TiO<sub>2</sub> quantum dots and LiPS that could adsorb soluble polysulfide compounds, leading to suppressing the shuttle effect. The interlayer also had abundant spacing and excellent conductivity because of the multiwalled carbon nanotube. The assembled LSB showed 1083 mAh g<sup>-1</sup> as the initial capacity and kept a cycle capacity of 610 mAh g<sup>-1</sup> after 600 cycles at a rate of 838 mAh g<sup>-1</sup>. Capacity decay rate was only 0.072% per cycle (Figure 15b) [125].

A superlight PP-coated film with multiwalled carbon nanotubes/nitrogen-doped carbon quantum dots (MWCNTs/NCQDs) was synthesized by Pang et al. (Figure 15c) [126]. The weight of the MWCNT/NCQD coating per area was as low as 0.15 mg cm<sup>-2</sup> (Figure 15d).

It was found to have superior capacity retention and self-discharge suppression compared to the LSB made by Chung et al. with an MWCNT-modified separator [127]. The synergistic influence of the MWCNTs and NCQDs was ultimately positive, resulting in 1331 mAh g<sup>-1</sup> as an initial capacity and presenting a stable cycling performance. The capacity decay was as low as 0.05% per cycle at 0.5 C, over 1000 cycles (Figure 15e).

Yu et al. developed a Mo<sub>2</sub>C quantum dot (MQD)-anchored nitrogen-doped graphene-deposited separator (MQD/NG) [128]. Figure 15f shows the optical and TEM pictures of the separator with MQD/NG/PP surface after 200 cycles. Polar Mo<sub>2</sub>C QDs offer a uniform lithium deposition and good chemical adsorption of LiPS. The LSB operated more than 1600 h with dendrite-free lithium deposition at a current density of 10 mA cm<sup>-2</sup>. The capacity of 1230 mAh g<sup>-1</sup> was observed under stable cycle performance after 100 cycles at 0.2 C without obvious capacity decay (Figure 15g).

Liu et al. developed a zinc sulfide quantum dot/reduced graphene aerogel-modified separator [126]. The ZnS quantum dots were effective as LiPS-anchoring and catalytic sites, which could promote the redox reaction of sulfur and mitigate the shuttle effect. The 3D porous reduced graphene aerogel assisted in physically blocking the migration of LiPS. As a consequence, 1211 mAh g<sup>-1</sup> at initial capacity was observed at 0.1 C and presented a stable cycling performance over 500 cycles at 1 C [129].

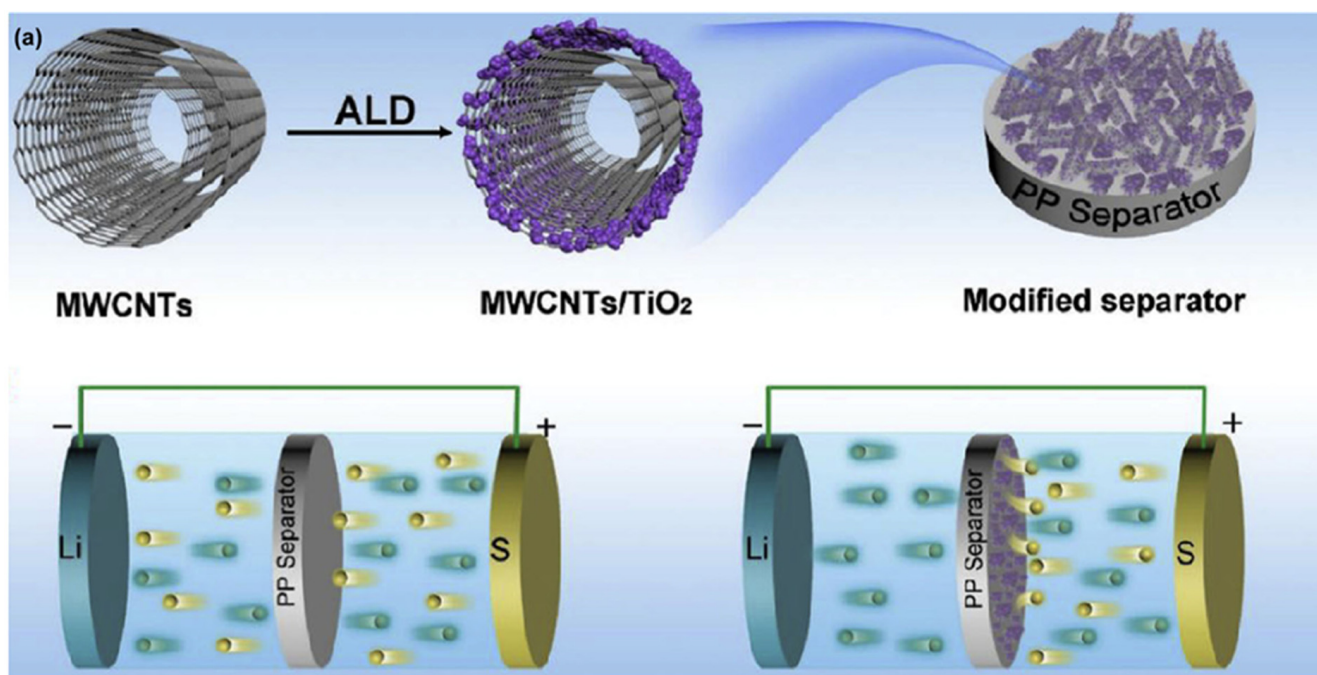
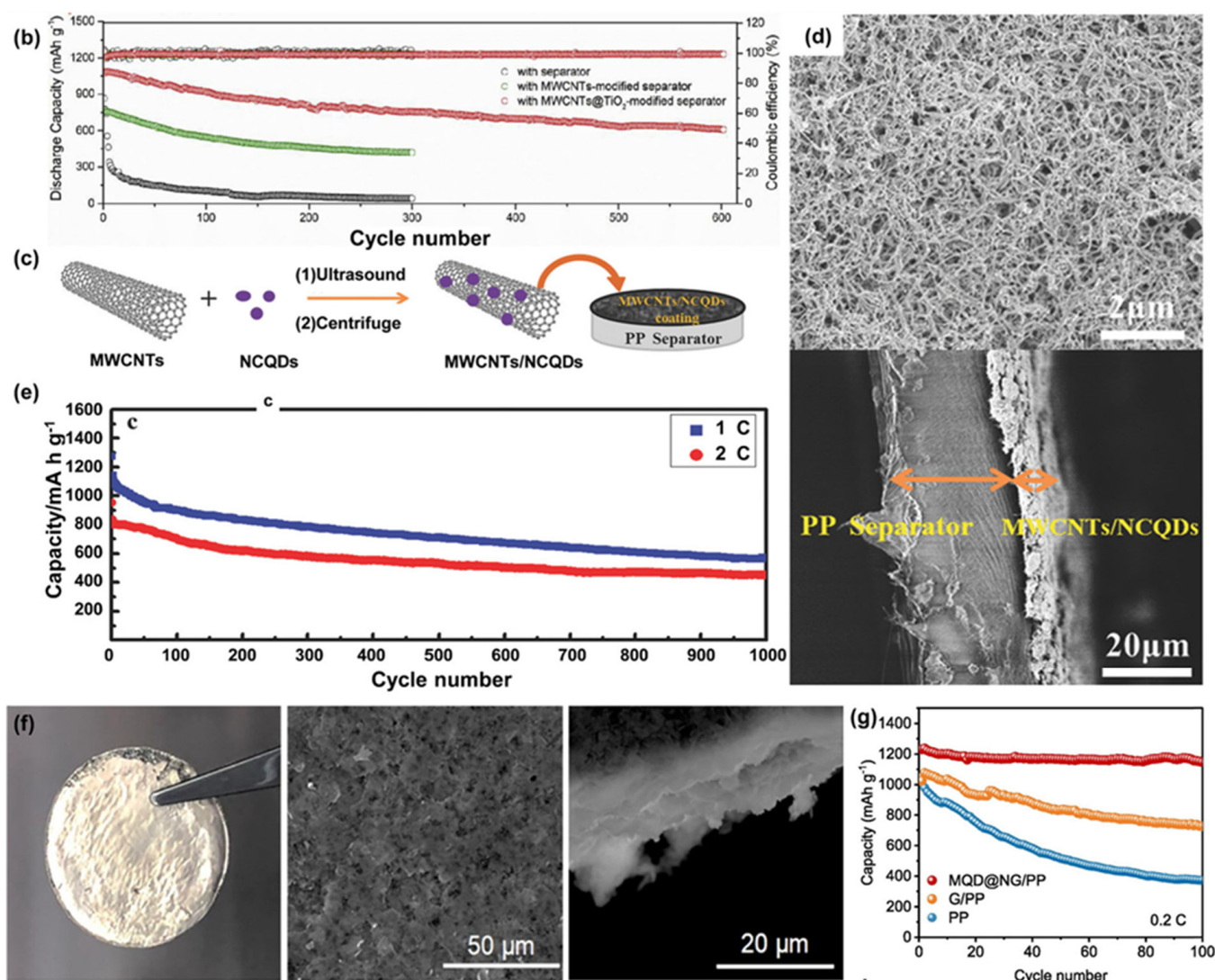


Figure 15. Cont.



**Figure 15.** (a) Speculated image of the synthesis procedure of MWCNTs/TiO<sub>2</sub> quantum dots and LSB with conventional PP and applied MWCNTs/TiO<sub>2</sub> quantum dots. (b) Cycle tests of LSB prepared with PP, MWCNTs/PP, and MWCNTs/TiO<sub>2</sub> quantum dots/PP. (c) Speculated image of MWCNTs/NCQDs composite and HRTEM picture of NCQDs anchored on MWCNTs surface. (d) SEM image of MWCNTs/NCQDs-applied separator and cross-sectional view of MWCNTs/NCQDs-applied separator. (e) Cycle test of the LSB assembled with MWCNTs/NCQDs-applied separator. (f) Digital and SEM image of lithium metal after plating/stripping experiments carried out with MQD/NG/PP separators for 200 cycles. (g) Cycle performance of LSB prepared with PP, G/PP, and MQD/NG/PP [125–128].

Zhang et al. applied MoP quantum dot and nitrogen, phosphorous co-doped polypyrrole (PPy) composite material to a commercial separator for LSBs [130]. The MoP quantum dots exhibited chemisorption and catalytic conversion performance for LiPS capture and conversion. In addition, N,P co-doped PPy substrates offered flexible pathways for Li<sup>+</sup>/electron transportation and also behaved as a physical barrier to mitigate the shuttling effect. The capacity of 739 mAh g<sup>-1</sup> at 3 C was observed with a stable cycle performance (600 mAh g<sup>-1</sup> at 1 C after 600 cycles, 0.052% decay per cycle). Density functional theory calculations elucidated that the MoP quantum dots possess enough adsorption energy for S<sub>8</sub> and Li<sub>2</sub>S<sub>n</sub>, which could lower the nucleation energy barrier of Li<sub>2</sub>S that might be helpful to accelerate Li<sub>2</sub>S reaction kinetics.

Cobalt aluminum-layered double-hydroxide quantum dots (LDH-QDs) was combined with nitrogen doped graphene (NG) as a coated material for LSB separator [125]. Experimental results and analysis, including XPS, clarified that the porous LDH-QDs/NG owned

rich active hydroxyl groups and  $\text{Co}^{2+}$  sites that were effective in catching LiPS through strong chemical interactions and promote the conversion reaction kinetics. The average thickness of the prepared LDH-QDs/NG-coated separator was approximately 17  $\mu\text{m}$  and had a high ionic conductivity of 2.67  $\text{mS cm}^{-1}$  [131].

#### 2.2.9. Separator Material: Mxenes

“MXenes” are materials known as two-dimensional transition metal carbides, nitrides, and carbonitrides and have been gaining significant attention owing to their high conductivity, rich functionality on Mxene surface, and exclusive two-dimensional morphologies, especially for energy storage devices [132,133].

Gogotsi et al. prepared  $\text{Ti}_3\text{C}_2$  by removing Al atoms selectively from layered hexagonal ternary carbide in 2011,  $\text{Ti}_3\text{AlC}_2$ , with hydrofluoric acid (HF) treatment in water [134]. This study focused on  $\text{Ti}_3\text{C}_2$  as a typical MXene material and prompted more researchers to investigate its physical and electrochemical properties [135,136]. In general, MXenes (such as  $\text{Ti}_3\text{C}_2\text{T}_x$  and  $\text{V}_2\text{CT}_x$ ) are two-dimensional layered materials, which can be obtained from transition metal carbides, nitrides, and carbonitrides (denoted as the MAX/ $\text{M}_{n+1}\text{AX}_n$  phase) [137]. These interesting materials can be acquired by selectively etching SP element layers from their corresponding three-dimensional MAX phases. MAX phases indicate layered ternary metal carbides, nitrides, or carbonitrides, with a formula of  $\text{M}_n + 1\text{AX}_n$  ( $n = 1, 2, 3$ ), in which M, A, and X express early d-block transition metals, main group SP elements, and either or both C and N atoms, respectively. Thus far, more than 70 MAX phases have been reported [138]. Typical MXene are  $\text{Ti}_3\text{C}_2$  [139],  $\text{Ti}_2\text{C}$  [140],  $(\text{Ti}_{0.5}, \text{Nb}_{0.5})_2\text{C}$ ,  $(\text{V}_{0.5}, \text{Cr}_{0.5})_3\text{C}_2$ ,  $\text{Ti}_3\text{CN}$  [141],  $\text{Ta}_4\text{C}_3$ ,  $\text{Nb}_2\text{C}$ ,  $\text{V}_2\text{C}$ , and  $\text{Nb}_4\text{C}_3$ , etc. Additional interesting properties of Mxene is that the surfaces generally terminate with F, OH, and/or O groups. Therefore, these terminated MXene species will be regarded as  $\text{M}_n + 1\text{X}_n\text{T}_x$ , in which T indicates the surface groups (F, OH, and/or O) and “x” is the number of terminations [142]. These surface groups can also assist in capturing LiPS diffusion.

Glass fiber and  $\text{Ti}_3\text{C}_2$  composite separator were prepared by Lin et al. via a vacuum filtration process [143]. As displayed in Figure 16a, a few layers of a conductive  $\text{Ti}_3\text{C}_2$  nanosheet with an average thickness of 1–4 nm were deposited on a glass fiber separator. This type of separator can offer strong LiPS adsorbing sites due to their high porosity, and LiPSs shuttle effect was successfully reduced when compared to a glass fiber separator without Mxene. The LSB assembled with Mxene/glass fiber composite separator offered a capacity of 820  $\text{mAh g}^{-1}$  at initial cycle and it was 721  $\text{mAh g}^{-1}$  after 100 cycles at 0.5 A  $\text{g}^{-1}$ , that is approximately 15 times stronger than LSBs with commercial separators (Figure 16b). High performance was achieved due to its conductive property and the strong interaction of  $\text{Ti}_3\text{C}_2$  toward LiPS.

$\text{TiO}_2$ -MXene heterostructures were prepared by Jiao et al. via the partial oxidation of  $\text{Ti}_3\text{C}_2\text{T}_x$  nanosheets [144]. It was shown that this crafted structure had a large surface area, strong ability to catch LiPS, and high conductivity and electrocatalytic activity. Figure 16c depicts how  $\text{TiO}_2$  uniformly distributed over MXene sheets can offer numbers of effective adsorbing sites to catch LiPS, while its heterostructure interface assures the rapid diffusion of LiPS to MXene, leading to its high catalytic activity for rapid LiPS conversion. The discharge capacity of LSB assembled with this  $\text{TiO}_2$ -MXene-deposited separator was 662  $\text{mAh g}^{-1}$  after 200 cycles at 0.5 C, which indicates 93% of capacity retention, proving its high sulfur utilization efficiency (Figure 16d).

MXene sulfation has also been studied. Yao et al. developed a flexible, conductive MXene ( $\text{Ti}_3\text{C}_2\text{T}_x$ ) sandwich-structured layer, and the heterostructure surface of  $\text{TiS}_2/\text{TiO}_2$  was created via vulcanization [145]. The  $\text{TiO}_2$  nanoparticles worked as an adsorbent to catch LiPSs and the  $\text{TiS}_2$  functioned as a catalyst to accelerate the long-chain LiPSs conversion to short-chain  $\text{Li}_2\text{S}_2/\text{Li}_2\text{S}$ , with the help of the high conductivity of  $\text{Ti}_3\text{C}_2\text{T}_x$ . It was found that the prepared layer protected the lithium anode by suppressing LiPS depositing on its surface. As a result, the long-term stability of a high electrochemical performance was achieved (capacity decay rate was 0.048% per cycle up to 500 cycles at 1 C).

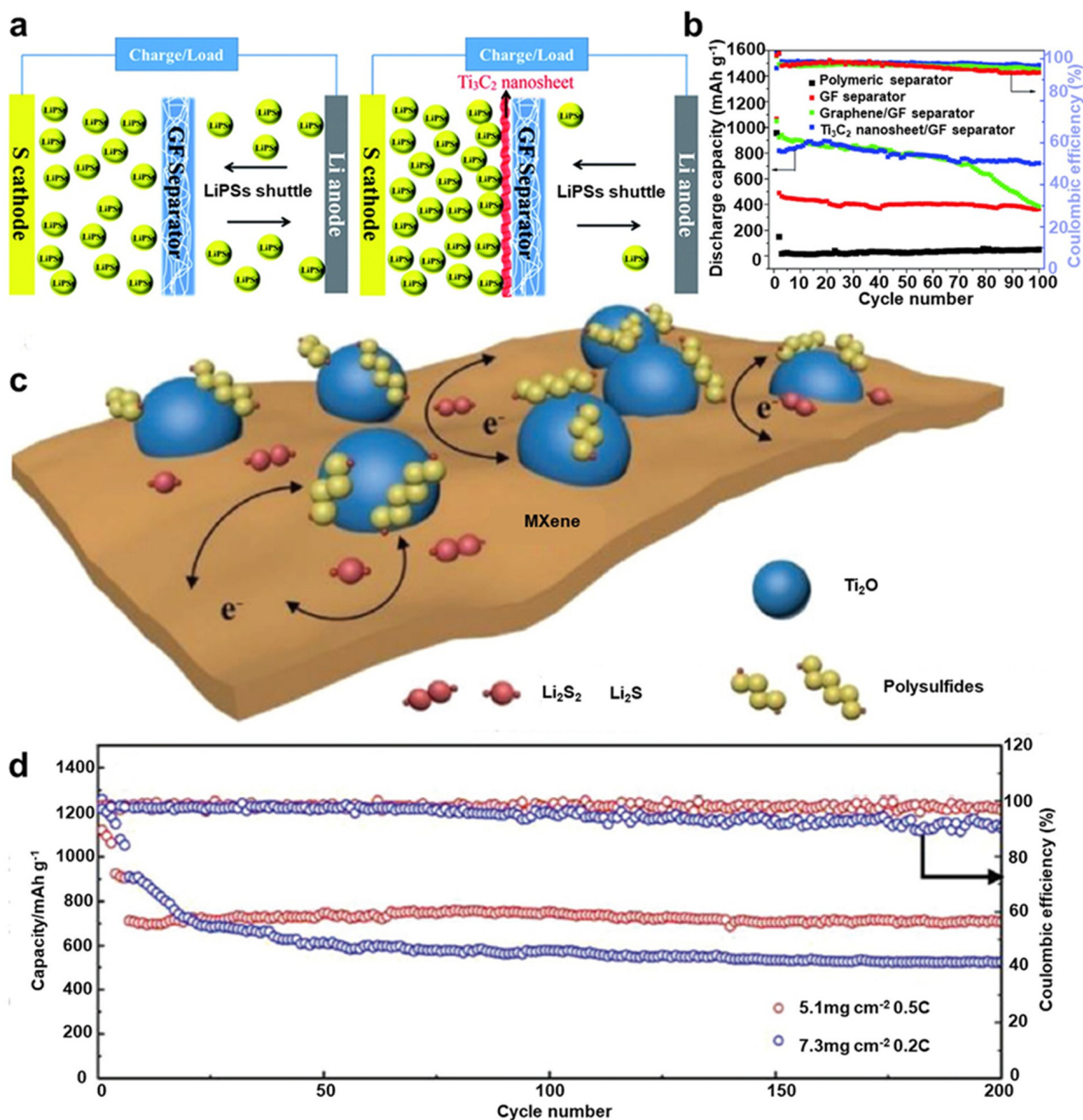


**Figure 16.** (a) Speculated image of the cell with a GF or GF/Ti<sub>3</sub>C<sub>2</sub> separator. (b) Cycling performance and coulombic efficiency at 0.5 A g<sup>-1</sup>. (c) Speculated image of the LiPS capture and process on TiO<sub>2</sub>-Ti<sub>3</sub>C<sub>2</sub>T<sub>x</sub> structures. (d) Cycling performance of LSBs with a Ti<sub>3</sub>C<sub>2</sub>T<sub>x</sub>-GN with different amounts of sulfur loadings [143,144].

Mxene has been combined with other functional materials to create even more desirable separators. Covalent organic frameworks (COFs) obtained with guanidinium salts have been gaining increasing attention as they possess strong covalent bonds and rich pore channels. It was suggested that guanidinium salts could capture LiPS, owing to their electrostatic interaction nature. Li et al. prepared ionic covalent organic nanosheets with guanidinium salts to prevent Ti<sub>3</sub>C<sub>2</sub> restacking and capturing LiPS. This material was uniformly applied to a polymer separator with a simple vacuum filtration process. The charge transfer resistance of LSB assembled with this type of separator was low so as to demonstrate good performance [146].

Combining Mxene with functional polymers can be a useful way to facilitate  $\text{Li}^+$  transport. Wang et al. prepared a laminar Nafion–MXene composite [147]. Interestingly, Nafion worked as a surfactant, or dispersant, which led to obtaining an ordered-structured MXene. When this composite was compared to each Nafion and MXene material, the shuttle effect was mitigated. LSB made with this functional separator exhibited good stability, and the capacity decay was as low as 0.03% per cycle over 1000 cycles. It was also found that the MXene promoted the reutilization of polysulfides, owing to its high electrical conduction, and an effective  $\text{Li}^+$  transport was achieved by Nafion.

#### 2.2.10. Other Functional Separator Materials

There are some additional functional materials that are being researched for use as LSB separators that either demonstrate the ability to capture LiPS to suppress the shuttle effect or provide catalytic sites to promote the redox reaction of sulfur-related species.

He et al. developed vanadyl phosphate ( $\text{VOPO}_4$ ) sheets for such a purpose [148]. Specifically, two-dimensional  $\text{VOPO}_4$  sheets with rich active sites were designed to adsorb LiPS through V–S bond formation. Due to the intrinsic electrical repulsion between the polysulfide anions, advanced time/space-resolved operando Raman analysis revealed that polysulfides' rich surfaces could further evolve to a "polysulfide-phobic" interface. By implementing these "polysulfide-phobic" sites in the separator, the LSB would have superior long-term cycling stability.

Pure Nafion, i.e., without Mxene, was coated onto a commercial separator by Huang et al. [149] in order to create ion selectivity.  $\text{SO}_3^-$  groups in sulfonate-ended perfluoroalkyl ether groups in separators allowed for  $\text{Li}^+$  hopping as a positively charged species, but did not allow for the hopping of negative ions, such as polysulfide anions ( $\text{S}_n^{2-}$ ), due to coulombic interactions. This cation-selective membrane worked as an effective electrostatic shield for polysulfide anions and succeeded in confining the LiPS to the cathode side.

Some nature-derived materials have also been studied. A lignin nanoparticle-coated commercial separator was prepared by Zhang et al. [150]. The lignin-coated separator had abundant electron-donating groups and was expected to result in the chemical binding of LiPS to reduce the shuttle effect. With an LSB, a cathode composed of sulfur and commercially available acetylene black (approximately 73.8 wt% sulfur content) was assembled and showed improved cycling stability compared to a commercial separator for over 500 cycles at a current density of 1 C.

Cellulose is another abundant and environmentally friendly organic resource and can be obtained from plant biomass. Nano-fibrillated cellulose (NFC) has been used to prepare porous natural separator membranes with a process learned from the paper industry. A separator composed of NFC was investigated regarding its porosity, thickness, wettability, and electrochemical stability, and its electrochemical performance as a functional separator for an LSB was evaluated. Interestingly, the mass of the commercial separator and the thinnest separator prepared in their study were very similar, although the cellulose-based separator was thicker. Top-down views of the NFC\_20PO (the separator prepared by adding paraffin oil and polyethylene glycol hexadecyl ether as a surfactant) and NFC\_20 (the separator prepared without any additive in water dispersion) are shown in Figure 16. The NFC\_20PO (Figure 17a) separator has an open-pore structure with interconnected pores of diameters between 100 nm and 1  $\mu\text{m}$ . The addition of PO and surfactant enabled the formation of pores; however, some parts remained partially closed, which implies that the preparation procedure is still not fully optimized. In contrast, the separator prepared without additives showed a much more closed, densely packed surface without any visible macro-pore structure (Figure 17b). It was suggested that the NFC fibers tend to compactly collapse from capillary action during the evaporation of water and are fixed with strong hydrogen bonds of cellulose chains, thus yielding dense-structured membranes [151]. It was also demonstrated that the electrochemical performance of the NFC separator was superior to the conventional polyolefin separator [152].

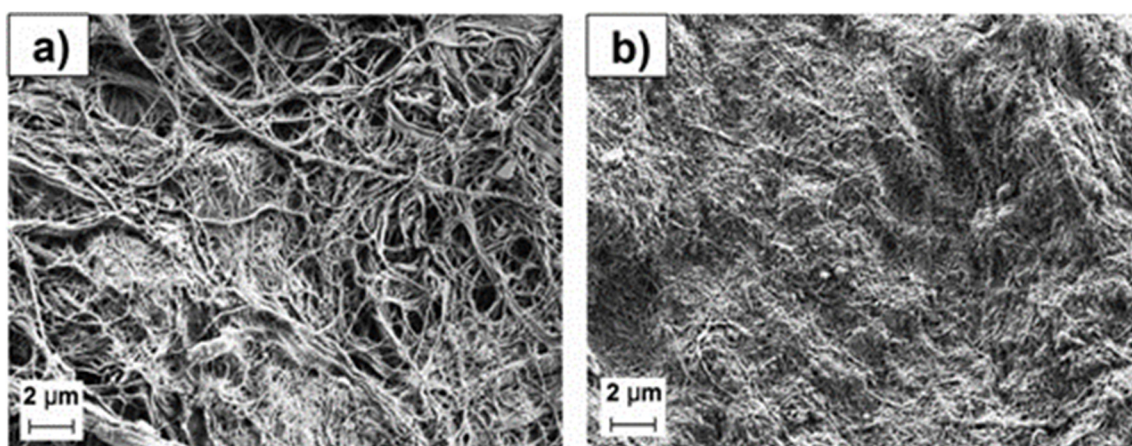


**Figure 17.** Morphology of the surface of separators prepared from water dispersion [152] (a) containing NFC (nano-fibrillated cellulose) fiber, paraffin oil, and surfactant; and (b) containing only NFC fibers.

It should be mentioned here that various types of materials were applied as LSB separators, as described so far, and are classified based on whether they are on the anode or cathode side of the separator. However, despite the explanation based on which side of the separator they are applied, some of them are applied on both sides of the separator. We explain this by emphasizing that the applied material acts as a functional material on a particular side. One such example, which clearly states that the  $\text{MnO}_2$  functional layers are on both the anode and cathode sides, is the study of Tian et al., who demonstrated that  $\text{MnO}_2$  was able to suppress LiPS migration with its chemical adsorption ability, which resulted in improving LSB electrochemical performance [153].

In addition, all of the materials applied to LSB separators in this study are summarized in Tables 1 and 2, depending upon whether they are on the anode or cathode side. One of the major roles for these separator materials are to capture LiPS in order to suppress the shuttle effect. Furthermore, the applied materials with both lithium polysulfide adsorption and catalytic activities are presented in Table 3 as multifunctional materials.

**Table 1.** Comparative performances of LSB with various types of materials on separator anode side.

Materials on Separator	Current Density (C, 1675 mAh g <sup>-1</sup> )	Cycle Number	Initial Discharge Capacity (mAh g <sup>-1</sup> )	Capacity Retention (%) (Fading Rate)	Reference
Metal					
Mg nanoparticles		400	135–140	80	[39]
Silver	0.5	300	131	92	[40]
Ceramic					
Boron Nitride	4	250	1018	69	[43]
SiO <sub>2</sub> Nanotubes	0.5	100	1266		[44]
Hollow Porous SiO <sub>2</sub> Nanocubes	100 mAh g <sup>-1</sup>	30	919 (30th)		[45]
SiO <sub>2</sub>	0.2	200	956.3	36	[47]
Al <sub>2</sub> O <sub>3</sub>	0.2	100	1067.7	75	[48]
Other Functional Materials					
polypyrrole	0.5	250		(0.083% per cycle)	[52]
porphyrin-derived graphene	0.5	300		(0.099% per cycle)	[56]
lithium fluoride	0.2	200		69.30%	[57]

**Table 2.** Comparative performances of LSB with various types of materials on separator cathode side.

Materials on Separator	Current Density (C, 1675 mAh g <sup>-1</sup> )	Cycle Number	Initial Discharge Capacity (mAh g <sup>-1</sup> )	Capacity Retention (%) (Fading Rate)	Reference
Carbonaceous Materials					
Ketjen black	0.1	100	1318		[60]
carbon	0.1	200	1112	63.8	[62]
carbon nanotube	0.5	400	1056	(0.11% per cycle)	[63]
Graphene Composite	2	1000	707	74.0%	[69]
nitrogen-doped reduced GO/Co-Ni-S composite	0.1	350	1524		[74]
nitrogen and sulfur doped carbon	2	500	841 (0.1C)	(0.089% per cycle)	[76]
Fe, nitrogen-doped carbon nanofibers and 2D graphene	0.5	500	847.9	(0.053% per cycle)	[77]
Metal Oxide					
Al <sub>2</sub> O <sub>3</sub>	0.2	50	967	70.0%	[78]
TiO <sub>2</sub> /carbon composite	0.1	150	926	75.0%	[79]
TiO <sub>2</sub> modified carbon nanotubes	0.5	900	1103.9	(0.066% per cycle)	[80]
SiO <sub>2</sub>	0.2	200	956.3	64.0%	[81]
CoSe <sub>2</sub> /grapheme oxide	6	500	916	50.1%	[84]
Lanthanum oxide	1	200	966	74.5%	[85]
Metal Sulfide					
reduced Graphene Oxide@MoS <sub>2</sub>	0.5	500	1122	0.116% per cycle	[86]
MoS <sub>2</sub> /C hollow microsphere	1	1000	935	(0.053% per cycle)	[88]
ZnS nanosheet/graphene	0.1	100	1165.9	58.8%	[89]
WS <sub>2</sub> Prussian Blue-Polypyrrole		300	1050	62.0%	[91]
Metal Carbide					
TiC-TiO <sub>2</sub>	1	500	1218	58.6%	[93]
WC/reduced Graphene Oxide composite	1	300		83.0%	[97]
Co <sub>3</sub> W <sub>3</sub> Carbide@C	1 A g <sup>-1</sup>	500		(0.06% per cycle)	[98]
NbC	5	1500		(0.037% per cycle)	[99]
Metal Nitride					
MoN <sub>x</sub>	0.1	500	1298	(0.063% per cycle)	[102]
BN Nanotube	0.3	200	1429		[103]
Co-doped g-C <sub>3</sub> N <sub>4</sub>	0.2	100	1121	95.0%	[105]
Phosphide					
CoP nanosphere	1	500		(0.078% per cycle)	[107]
CoP/C	1	500	938	(0.08% per cycle)	[108]
FeP/C	1	400	526		[109]
Ni/Ni <sub>2</sub> P-Carbon	5	1500	431	(0.031% per cycle)	[110]
Metal Organic Framework					
Ce UiO-67	1	500	919	0.04%/cycle	[119]
Ce-UiO-66-NH <sub>2</sub>	0.2	300	1366.3	0.09%/cycle	[120]
ZIF-8	0.1	199	1235.6		[121]
Quantum Dot					
TiO <sub>2</sub> Quantum Dot		600	1083	0.072%/cycle	[125]
MWCNT/Nitrogen Doped Carbon Quantum Dot	0.5	1000	1330.8	0.05%/cycle	[126]

Table 2. Cont.

Materials on Separator	Current Density (C, 1675 mAh g <sup>-1</sup> )	Cycle Number	Initial Discharge Capacity (mAh g <sup>-1</sup> )	Capacity Retention (%) (Fading Rate)	Reference
Mo2C quantum dot	0.2	100	1230		[128]
ZnS Quantum Dot	0.1	500	1211		[129]
MoP Quantum Dot	1	600	500	0.052%/cycle	[130]
Mxene					
Ti3C2		100	820	0.879%/cycle	[143]
TiO2-Ti3C2Tx	0.5	200	662	0.035 %/cycle	[144]
TiS2/TiO2-Ti3C2Tx	1	500		0.048 %/cycle	[145]
Other Functional Materials					
Lignin	1	500	487		[150]
Nano-fibrillated cellulose	1		580		[152]

Table 3. Comparative performances of LSB with various types of materials with both lithium polysulfide adsorption and catalytic activities.

Materials on Separator	Current Density (C, 1675 mAh g <sup>-1</sup> )	Cycle Number	Initial Discharge Capacity (mAh g <sup>-1</sup> )	Capacity Retention (%) (Fading Rate)	Reference
Lanthanum oxide	1	200	966	74.5%	[85]
Co <sub>3</sub> W <sub>3</sub> Carbide@C	1	500		(0.06% per cycle)	[92]
Co-doped g-C <sub>3</sub> N <sub>4</sub>	0.2	100	1121	95.0%	[99]
FeP/C	1	400	526		[109]
Ni/Ni <sub>2</sub> P-Carbon	5	1500	431	(0.031% per cycle)	[110]
MOF and MOF Composite					[113]
ZnS Quantum Dot	0.1	500	1211		[126]
MoP Quantum Dot	1	600	500	0.052%/cycle	[130]
TiO <sub>2</sub> -Mxene					[144]

Each material has advantages and disadvantages. In addition, for future study, combining these materials and creating composite materials could also be another strategy to gain even better performance.

### 3. Necessary Properties for LSB Separators

We have explained the actual materials for which attempts have been made to apply them to LSB separators so far. Now, we would like to further discuss the necessary properties for LSB separators.

In general, electronic resistance and ion conductivity need to be high for LSB separators. Ionic conductivity is related to separator structure, including porosity and tortuosity. Porosity is necessary to save enough electrolytes in order to keep ionic transference in an enhanced level. Tortuosity is an additional important factor. Tortuosity is the amount to explain the morphology. As tortuosity becomes smaller, conductivity will be higher. Furthermore, wettability is also a key factor to determine ionic conductivity. Obviously, a higher electrolyte permeation could serve as an easier way for lithium ion transportation. It should also be noted that the pore size and tortuosity should be uniform in order to obtain stable current density [154].

#### 3.1. Separator Porosity, Pore Size, and Thickness

In general, a thinner separator should possess reduced ionic resistance, which would result in gaining a higher energy density. So far, separator thickness ranges within 20–50 μm,

whereas that of commercial separator thickness is 20–25  $\mu\text{m}$  [155]. A thinner separator tends to be more fragile, which would be the reason for short circuits and explosions. The uniformity and equality of thickness can be critical because an uneven separator can be the reason for dendrite formation, which would cause disaster during battery operation.

In addition, separator porosity can be expressed by the following equation:

$$\text{Porosity (\%)} = (1 - \rho_m/\rho_p) \times 100 \quad (2)$$

where  $\rho_m$  is the apparent density and  $\rho_p$  is the density of the separator material [156].

In general, the porosity is calculated by the weight difference before and after separator immersion in the liquid, as shown in the equation:

$$\text{Porosity (\%)} = W - w_0/\rho_L V_0 \quad (3)$$

where  $W$  is the intact separator weight and  $w_0$  is the weight of the separator after liquid immersion;  $\rho_L$  and  $V_0$  denote the liquid density and the separator volume, respectively.

Porosity needs to be optimized so that electrolytes are filled in the pores to assure ion conductivity. For example, the separator itself would be weak if porosity is too high. In contrast, if the porosity is too small, ion conductivity would not be high enough to ensure good electrochemical performance. The optimized porosity of separators for a commercial lithium ion battery is known to be approximately 40%, and that of lithium sulfur battery is still controversial, since there are not as many commercialized lithium sulfur batteries in number [157].

### 3.2. Tortuosity and Permeability

Tortuosity for a separator can be a factor indicating the influence of the separator shape upon the ionic conductivity [158], and can be expressed by the following equation:

$$\tau = \sqrt{\varepsilon \times R_s/R_0} \quad (4)$$

where  $\varepsilon$  is the porosity,  $R_s$  and  $R_0$  are the separator resistance before and after being soaked in liquid electrolyte, respectively.

Geometric effective transport coefficient can be a measure of the effective ionic transport of separators' morphology, and can be calculated as  $\delta = \varepsilon/\tau$ .

The permeability is similar to tortuosity. Geometric structure can influence the ionic conductivity by pressure difference and the permeability can be applied in this respect.

Darcy's law can be applied to define the rate of the fluid through the porous surface, which can be expressed by the following equation:

$$u = -\kappa/\eta \nabla P \quad (5)$$

where  $\eta$  is the viscosity,  $\nabla P$  is the applied pressure gradient, and  $u$  is the average velocity of the fluid when penetrating the porous surface [159].

### 3.3. Wettability

Wettability is also one of the critical factors because it influences the electrolyte absorption. When wettability is high, one can say that the separators' resistance becomes small, which would be ideal for the LSB performance [160]. It is also known that wettability is related to the porosity, pore size, morphology, and characteristics of each separator.

### 3.4. Mechanical Properties and Thermal Behavior

Mechanical strength is necessary for separators to suppress the dendrite growth and short circuit. Tensile and puncture strength are the most important mechanical properties. Particularly, high tensile strength is necessary in the stretched directions for separators, whereas the puncture strength is the weight which is necessary for a needle to make a puncture on the separator [158]. Puncture strength has been applied to define how hard

separators can bear a short circuit during battery assembly, manufacture, and electrochemical reactions. Sufficient puncture strength is necessary to confirm that separators do not break, or otherwise, a short circuit will occur, which would cause critical damage to the battery. The separator should also not deform or shrink because of temperature rise.

In summary, even though there are many strategies and candidate materials for separators, which may improve the LSB electrochemical performance, the abovementioned characteristics, such as separator thickness, porosity (pore size), tortuosity, electrolyte wettability, and permeability, need to be carefully considered when selecting the materials. Moreover, the mechanical strength of a separator is also important. In brief, one has to choose good separator materials and they need to be optimized to achieve high LSB performance.

The author group of this article also successfully improved the LSB electrochemical performance by optimizing the cathode materials and composition, electrolyte composition, and separator. The separator was coated with a metal organic framework-derived ink to enhance its LiPS-capturing ability [115,117,161]. Details will be described in a forthcoming paper.

#### 4. Conclusions

In summary, it is necessary to think about whether an applied material on a separator is facing the anode or cathode side because of the different roles the orientation plays. The main roles of a separator are to adsorb LiPS to suppress the shuttle effect, boost catalytic activity to promote the sulfur-based redox reaction, function as a physical or chemical barrier to minimize LiPS migration from the cathode to the anode, and provide lithium affinity to control the lithium metal dendrite growth on the anode. For these purposes, materials such as metals, carbonaceous materials, oxides, nitrides, carbides, metal organic frameworks, quantum dots, Mxenes, biomass-derived lignins, and cellulose have all been studied. One also needs to remember that it is important to optimize necessary characteristics such as thickness, porosity, electrolyte permeability, and mechanical strength for separators to obtain high LBS performance. Each material and mechanism has its own merits and demerits and these intensive research efforts are necessary to improve the electrochemical properties of LSBs.

**Funding:** This research received no external funding.

**Institutional Review Board Statement:** Not applicable.

**Informed Consent Statement:** Not applicable.

**Data Availability Statement:** The data presented in this study are available on request from the corresponding author.

**Acknowledgments:** The author wishes to thank Hideki Yoshioka, Katsuji Konishi, Yoishi Inubushi, and Yoshiyuki Nakano for their helpful discussions.

**Conflicts of Interest:** Author Ryohei Mori was employed by the company Green Science Alliance Co., Ltd. and Fuji Pigment Co., Ltd. The author declares that the research was conducted in the absence of any commercial or financial relationships that could be construed as a potential conflict of interest.

#### References

1. Kim, T.; Song, W.; Son, D.Y.; Ono, L.K.; Qi, Y. Lithium-ion batteries: Outlook on present, future, and hybridized technologies. *J. Mater. Chem. A* **2019**, *7*, 2942–2964. [[CrossRef](#)]
2. Manthiram, A. A reflection on lithium-ion battery cathode chemistry. *Nat. Commun.* **2020**, *11*, 1550. [[CrossRef](#)] [[PubMed](#)]
3. Etacheri, V.; Marom, R.; Elazari, R.; Salitra, G.; Aurbach, D. Challenges in the development of advanced Li-ion batteries: A review. *Energy Environ. Sci.* **2011**, *4*, 3243–3262. [[CrossRef](#)]
4. Xu, G.; Ding, B.; Pan, J.; Nie, P.; Shen, L.; Zhang, X. High performance lithium-sulfur batteries: Advances and challenges. *J. Mater. Chem. A* **2014**, *2*, 12662–12676. [[CrossRef](#)]

5. Kang, W.; Deng, N.; Ju, J.; Li, Q.; Wu, D.; Ma, X.; Li, L.; Naebe, M.; Cheng, B. A review of recent developments in rechargeable lithium–sulfur batteries. *Nanoscale* **2016**, *8*, 16541–16588. [[CrossRef](#)]
6. Lopez, C.V.; Maladeniya, C.P.; Smith, R.C. Lithium-sulfur batteries: Advances and trends. *Electrochem* **2020**, *1*, 226–259. [[CrossRef](#)]
7. Manthiram, A.; Fu, Y.; Chung, S.H.; Zu, C.; Su, Y.S. Rechargeable lithium–sulfur batteries. *Chem. Rev.* **2014**, *114*, 11751–11787. [[CrossRef](#)]
8. Li, G.; Li, Z.; Zhang, B.; Lin, Z. Developments of electrolyte systems for lithium–sulfur batteries: A review. *Front. Energy Res.* **2015**, *3*, 1. [[CrossRef](#)]
9. Guo, J.; Liu, J. A binder-free electrode architecture design for lithium–sulfur batteries: A review. *Nanoscale Adv.* **2019**, *1*, 2104–2122. [[CrossRef](#)]
10. Yang, Y.; Zheng, G.; Cui, Y. A membrane-free lithium/polysulfide semi-liquid battery for large-scale energy storage. *Energy Environ. Sci.* **2013**, *6*, 1552. [[CrossRef](#)]
11. Zhang, S.S.; Read, J.A. A new direction for the performance improvement of rechargeable lithium/sulfur batteries. *J. Power Sources* **2012**, *200*, 77–82. [[CrossRef](#)]
12. Barchasz, C.; Molton, F.; Duboc, C.; Leprêtre, J.C.; Patoux, S.; Alloin, F. Lithium/sulfur cell discharge mechanism: An original approach for intermediate species identification. *Anal. Chem.* **2012**, *84*, 3973–3980, Corrigendum in **2020**, *92*, 13610. [[CrossRef](#)] [[PubMed](#)]
13. Yamaki, J.I.; Tobishima, S.I.; Sakurai, Y.; Saito, K.I.; Hayashi, K. Safety evaluation of rechargeable cells with lithium metal anodes and amorphous V<sub>2</sub>O<sub>5</sub> cathodes. *J. Appl. Electrochem.* **1998**, *28*, 135–140. [[CrossRef](#)]
14. Cao, R.; Xu, W.; Lv, D.; Xiao, J.; Zhang, J.G. Anodes for rechargeable lithium–sulfur batteries. *Adv. Energy Mater.* **2015**, *5*, 1402273. [[CrossRef](#)]
15. Brieske, D.M.; Warnecke, A.; Sauer, D.U. Modeling the volumetric expansion of the lithium-sulfur battery considering charge and discharge profiles. *Energy Storage Mater.* **2023**, *55*, 289–300. [[CrossRef](#)]
16. Kamisan, A.I.; Kudin, T.I.T.; Kamisan, A.S.; Omer, A.F.C.; Taib, M.F.M.; Hassan, O.H.; Ali, A.M.M.; Yahya, M.Z.A. Recent advances on graphene-based materials as cathode materials in lithium–sulfur batteries. *Int. J. Hydrogen Energy* **2022**, *47*, 8630–8657. [[CrossRef](#)]
17. Choi, Y.J.; Chung, Y.D.; Baek, C.Y.; Kim, K.W.; Ahn, H.J.; Ahn, J.H. Effects of carbon coating on the electrochemical properties of sulfur cathode for lithium/sulfur cell. *J. Power Sources* **2008**, *184*, 548–552. [[CrossRef](#)]
18. Ji, X.; Lee, K.T.; Nazar, L.F. A highly ordered nanostructured carbon–sulfur cathode for lithium–sulfur batteries. *Nat. Mater.* **2009**, *8*, 500–506. [[CrossRef](#)]
19. Liu, X.; Huang, J.Q.; Zhang, Q.; Mai, L. Nanostructured metal oxides and sulfides for lithium–sulfur batteries. *Adv. Mater.* **2017**, *29*, 1601759. [[CrossRef](#)]
20. Guo, Y.; Zhang, Y.; Zhang, Y.; Xiang, M.; Wu, H.; Liu, H.; Dou, S. Interwoven V<sub>2</sub>O<sub>5</sub> nanowire/graphene nanoscroll hybrid assembled as efficient polysulfide-trapping-conversion interlayer for long-life lithium sulfur batteries. *J. Mater. Chem. A* **2018**, *6*, 19358–19370. [[CrossRef](#)]
21. Hu, N.; Lv, X.; Dai, Y.; Fan, L.; Xiong, D.; Li, X. SnO<sub>2</sub>/reduced graphene oxide interlayer mitigating the shuttle effect of Li–S batteries. *ACS Appl. Mater. Interfaces* **2018**, *10*, 18665–18674. [[CrossRef](#)] [[PubMed](#)]
22. Cho, J.; Ryu, S.; Gong, Y.J.; Pyo, S.; Yun, H.; Kim, H.; Lee, J.; Yoo, J.; Kim, Y.S. Nitrogen-doped MoS<sub>2</sub> as a catalytic sulfur host for lithium–sulfur batteries. *Chem. Eng. J.* **2022**, *439*, 135568. [[CrossRef](#)]
23. Zhong, Y.; Xia, X.; Shi, F.; Zhan, J.; Tu, J.; Fan, H.J. Transition metal carbides and nitrides in energy storage and conversion. *Adv. Sci.* **2016**, *3*, 1500286. [[CrossRef](#)]
24. Gao, J.; Lowe, M.A.; Kiyu, Y.; Abruna, H.D. Effects of liquid electrolytes on the charge-discharge performance of rechargeable lithium/sulfur batteries: Electrochemical and in-situ X-ray absorption spectroscopic studies. *J. Phys. Chem. C* **2011**, *115*, 25132–25137. [[CrossRef](#)]
25. Zhang, S.S. Liquid electrolyte lithium/sulfur battery: Fundamental chemistry, problems, and solutions. *J. Power Sources* **2013**, *231*, 153–162. [[CrossRef](#)]
26. Aurbach, D.; Pollak, E.; Elazari, R.; Salitra, G.; Kelley, C.S.; Affinito, J. On the surface chemical aspects of very high energy density, rechargeable Li-sulfur batteries. *J. Electrochem. Soc.* **2009**, *156*, A694. [[CrossRef](#)]
27. Fan, W.; Zhang, L.; Liu, T. Multifunctional second barrier layers for lithium–sulfur batteries. *Mater. Chem. Front.* **2018**, *2*, 235–252. [[CrossRef](#)]
28. Chang, C.H.; Chung, S.H.; Manthiram, A. Ultra-lightweight PANiNF/MWCNT-functionalized separators with synergistic suppression of polysulfide migration for Li–S batteries with pure sulfur cathodes. *J. Mater. Chem. A* **2015**, *3*, 18829–18834. [[CrossRef](#)]
29. Kong, W.; Yan, L.; Luo, Y.; Wang, D.; Jiang, K.; Li, Q.; Fan, S.; Wang, J. Ultrathin MnO<sub>2</sub>/graphene oxide/carbon nanotube interlayer as efficient polysulfide trapping shield for high-performance Li–S batteries. *Adv. Funct. Mater.* **2017**, *27*, 1606663. [[CrossRef](#)]
30. Huang, J.Q.; Zhang, Q.; Wei, F. Multi-functional separator/interlayer system for high-stable lithium–sulfur batteries: Progress and prospects. *Energy Storage Mater.* **2015**, *1*, 127–145. [[CrossRef](#)]
31. Fiedler, M.; Cangaz, S.; Hippauf, F.; Dörfler, S.; Abendroth, T.; Althues, H.; Kastel, S. Mechanistic Insights into the Cycling Behavior of Sulfur Dry-Film Cathodes. *Adv. Sustain. Syst.* **2023**, *7*, 2200439. [[CrossRef](#)]

32. Xu, J.; Shui, J.; Wang, J.; Wang, M.; Liu, H.-K.; Dou, S.X.; Jeon, I.-Y.; Seo, J.-M.; Baek, J.-B.; Dai, L. Sulfur–Graphene Nanostructured Cathodes via Ball-Milling for High-Performance Lithium–Sulfur Batteries. *ACS Nano* **2014**, *8*, 10920–10930. [[CrossRef](#)] [[PubMed](#)]
33. Li, X.; Gao, M.; Du, W.; Ni, B.; Wu, Y.; Liu, Y.; Shang, C.; Guo, Z.; Pan, H. A mechanochemical synthesis of submicron-sized Li<sub>2</sub>S and a mesoporous Li<sub>2</sub>S/C hybrid for high performance lithium/sulfur battery cathodes. *J. Mater. Chem. A* **2017**, *5*, 6471–6482. [[CrossRef](#)]
34. Younes, H.; Hong, H.; Peterson, G.P. A Novel Approach to Fabricate Carbon Nanomaterials–Nanoparticle Solids through Aqueous Solutions and Their Applications. *Nanomanuf. Metrol.* **2021**, *4*, 226–236. [[CrossRef](#)]
35. Li, J.; Xiao, Z.; Chen, A.; Zhang, W.; Zhu, D.; Jin, Y.; Mao, Q.; Wang, G.; He, J.; Xia, Y. Functionally modified polyolefin-based separators for lithium–sulfur batteries: Progress and prospects. *Front. Energy Res.* **2020**, *8*, 593640. [[CrossRef](#)]
36. Yan, J.; Liu, X.; Li, B. Capacity fade analysis of sulfur cathodes in lithium–sulfur batteries. *Adv. Sci.* **2016**, *3*, 1600101. [[CrossRef](#)]
37. Peng, H.J.; Huang, J.Q.; Cheng, X.B.; Zhang, Q. Review on high loading and high-energy lithium–sulfur batteries. *Adv. Energy Mater.* **2017**, *7*, 1700260. [[CrossRef](#)]
38. Deng, N.; Liu, Y.; Li, Q.; Yan, J.; Lei, W.; Wang, G.; Wang, L.; Liang, Y.; Kang, W.; Cheng, B. Functional mechanism analysis and customized structure design of interlayers for high performance Li–S battery. *Energy Storage Mater.* **2019**, *23*, 314–349. [[CrossRef](#)]
39. Liu, Y.; Xiong, S.; Wang, J.; Jiao, X.; Li, S.; Zhang, C.; Song, Z.; Song, J. Dendrite-free lithium metal anode enabled by separator engineering via uniform loading of lithiophilic nucleation sites. *Energy Storage Mater.* **2019**, *19*, 24–30. [[CrossRef](#)]
40. Zuo, Z.; Zhuang, L.; Xu, J.; Shi, Y.; Su, C.; Lian, P.; Tian, B. Lithiophilic silver coating on lithium metal surface for inhibiting lithium dendrites. *Front. Chem.* **2020**, *8*, 109. [[CrossRef](#)]
41. Yang, C.P.; Yin, Y.X.; Zhang, S.F.; Li, N.W.; Guo, Y.G. Accommodating lithium into 3D current collectors with a submicron skeleton towards long-life lithium metal anodes. *Nat. Comm.* **2015**, *6*, 8058. [[CrossRef](#)] [[PubMed](#)]
42. Li, Q.; Zhu, S.; Lu, Y. 3D Porous Cu Current Collector/Li-Metal Composite Anode for Stable Lithium-Metal Batteries. *Adv. Funct. Mater.* **2017**, *27*, 1606422. [[CrossRef](#)]
43. Kim, P.J.H.; Seo, J.; Fu, K.; Choi, J.; Liu, Z.; Kwon, J.; Hu, L.; Paik, U. Synergistic protective effect of a BN-carbon separator for highly stable lithium sulfur batteries. *NPG Asia Mater.* **2017**, *9*, e375. [[CrossRef](#)]
44. Favors, Z.; Wang, W.; Bay, H.H.; George, A.; Ozkan, M.; Ozkan, C. Stable cycling of SiO<sub>2</sub> nanotubes as high-performance anodes for lithium-ion batteries. *Sci. Rep.* **2014**, *4*, 4605. [[CrossRef](#)] [[PubMed](#)]
45. Yan, N.; Wang, F.; Zhong, H.; Li, Y.; Wang, Y.; Hu, L.; Chen, Q. Hollow porous SiO<sub>2</sub> nanocubes towards high-performance anodes for lithium-ion batteries. *Sci. Rep.* **2013**, *3*, 1568. [[CrossRef](#)] [[PubMed](#)]
46. Suriyakumar, S.; Stephan, A.M.; Angulakshmi, N.; Hassan, M.H.; Alkordi, M.H. Metal–organic framework@SiO<sub>2</sub> as permselective separator for lithium–sulfur batteries. *J. Mater. Chem. A* **2018**, *6*, 14623–14632. [[CrossRef](#)]
47. Fu, D.; Luan, B.; Argue, S.; Bereau, M.N.; Davidson, I.J. Nano SiO<sub>2</sub> particle formation and deposition on polypropylene separators for lithium-ion batteries. *J. Power Sources* **2012**, *206*, 325–333. [[CrossRef](#)]
48. Song, R.; Fang, R.; Wen, L.; Shi, Y.; Wang, S.; Li, F. A trilayer separator with dual function for high performance lithium–sulfur batteries. *J. Power Sources* **2016**, *301*, 179–186. [[CrossRef](#)]
49. Hou, T.Z.; Chen, X.; Peng, H.G.; Huang, J.Q.; Li, B.Q.; Zhang, Q.; Li, B. Design principles for heteroatom-doped nanocarbon to achieve strong anchoring of polysulfides for lithium–sulfur batteries. *Small* **2016**, *12*, 3283–3291. [[CrossRef](#)]
50. He, Y.; Wu, S.; Li, Q.; Zhou, H. Designing a multifunctional separator for high-performance Li–S batteries at elevated temperature. *Small* **2019**, *15*, 1904332. [[CrossRef](#)]
51. Huo, H.; Li, X.; Chen, Y.; Liang, J.; Deng, S.; Gao, X.; Doyle-Davis, K.; Li, R.; Guo, X.; Shen, Y.; et al. Bifunctional composite separator with a solid-state-battery strategy for dendrite-free lithium metal batteries. *Energy Storage Mater.* **2020**, *29*, 361–366. [[CrossRef](#)]
52. Li, Y.; Wang, W.; Liu, X.; Mao, E.; Wang, M.; Li, G.; Fu, L.; Li, Z.; Eng, A.Y.S.; Seh, Z.W.; et al. Engineering stable electrode-separator interfaces with ultrathin conductive polymer layer for high-energy-density Li–S batteries. *Energy Storage Mater.* **2019**, *23*, 261–268. [[CrossRef](#)]
53. Wang, L.; Yang, H.; Liu, X.; Zeng, R.; Li, M.; Huang, Y.; Hu, X. Constructing hierarchical tectorum-like α-Fe<sub>2</sub>O<sub>3</sub>/PPy nanoarrays on carbon cloth for solid-state asymmetric supercapacitors. *Angew. Chem. Int. Ed.* **2017**, *129*, 1125–1130. [[CrossRef](#)]
54. Feng, J.X.; Xu, H.; Ye, S.H.; Ouyang, G.; Tong, Y.X.; Li, G.R. Silica-polypyrrole hybrids as high-performance metal-free electrocatalysts for the hydrogen evolution reaction in neutral media. *Angew. Chem. Int. Ed.* **2017**, *56*, 8120–8124. [[CrossRef](#)] [[PubMed](#)]
55. Li, W.; Zhang, Q.; Zheng, G.; Seh, Z.W.; Yao, H.; Cui, Y. Understanding the role of different conductive polymers in improving the nanostructured sulfur cathode performance. *Nano Lett.* **2013**, *13*, 5534–5540. [[CrossRef](#)]
56. Kong, L.; Li, B.; Peng, H.; Zhang, R.; Xie, J.; Huang, J.; Zhang, Q. Porphyrin-derived graphene-based nanosheets enabling strong polysulfide chemisorption and rapid kinetics in lithium–sulfur batteries. *Adv. Energy Mater.* **2018**, *8*, 1800849. [[CrossRef](#)]
57. Li, C.; Zhang, P.; Dai, J.; Shen, X.; Peng, Y.; Zhang, Y.; Zhao, J. Rational method for improving the performance of lithium–sulfur batteries: Coating the separator with lithium fluoride. *ChemElectroChem* **2017**, *4*, 1535–1543. [[CrossRef](#)]
58. Wang, Y.; Ai, R.; Wang, F.; Hu, X.; Zeng, Y.; Hou, J.; Zhao, J.; Zhang, Y.; Zhang, Y.; Li, X. Research Progress on Multifunctional Modified Separator for Lithium–Sulfur Batteries. *Polymers* **2023**, *15*, 993. [[CrossRef](#)]
59. Zhou, G.; Li, L.; Wang, D.W.; Shan, X.Y.; Pei, S.; Li, F.; Cheng, H.M. A flexible sulfur-graphene-polypropylene separator integrated electrode for advanced Li–S batteries. *Adv. Mater.* **2015**, *27*, 641–647. [[CrossRef](#)]

60. Zhao, D.; Qian, X.; Jin, L.; Yang, X.X.; Wang, S.; Shen, X.; Yao, S.; Rao, D.; Zhou, Y.; Xi, X. Separator modified by Ketjen black for enhanced electrochemical performance of lithium–sulfur batteries. *RSC Adv.* **2016**, *17*, 13680–13685. [[CrossRef](#)]
61. Chung, S.H.; Manthiram, A. A polyethylene glycol-supported microporous carbon coating as a polysulfide trap for utilizing pure sulfur cathodes in lithium–sulfur batteries. *Adv. Mater.* **2014**, *26*, 7352–7357. [[CrossRef](#)] [[PubMed](#)]
62. Huang, Y.C.; Yen, Y.J.; Tseng, Y.H.; Chung, S.H. Module-designed carbon-coated separators for high-loading, high-sulfur-utilization cathodes in lithium–sulfur batteries. *Molecules* **2022**, *77*, 228. [[CrossRef](#)] [[PubMed](#)]
63. Ponraj, R.; Kannan, A.G.; Ahn, J.H.; Lee, J.H.; Kang, J.; Han, B.; Kim, D.W. Effective trapping of lithium polysulfides using a functionalized carbon nanotube-coated separator for lithium–sulfur cells with enhanced cycling stability. *ACS Appl. Mater. Interfaces* **2017**, *9*, 38445–38454. [[CrossRef](#)] [[PubMed](#)]
64. Wang, L.; Dong, Z.H.; Wang, D.; Zhang, F.X.; Jin, J. Covalent bond glued sulfur nanosheet-based cathode integration for long-cycle-life Li–S batteries. *Nano Lett.* **2013**, *13*, 6244–6250. [[CrossRef](#)] [[PubMed](#)]
65. Wang, L.; Wang, D.; Zhang, F.; Jin, J. Interface chemistry guided long-cycle life Li–S battery. *Nano Lett.* **2013**, *13*, 4206–4211. [[CrossRef](#)] [[PubMed](#)]
66. Chen, R.; Zhao, T.; Lu, J.; Wu, F.; Li, L.; Chen, J.; Tan, G.; Ye, Y.; Amine, K. Graphene-based three-dimensional hierarchical sandwich-type architecture for high-performance Li/S batteries. *Nano Lett.* **2013**, *13*, 4642–4649. [[CrossRef](#)]
67. Yu, X.; Joseph, J.; Manthiram, A. Suppression of the polysulfide-shuttle behavior in Li–S batteries through the development of a facile functional group on the polypropylene separator. *Mater. Horiz.* **2016**, *3*, 314–319. [[CrossRef](#)]
68. Vizintin, A.; Lozinšek, M.; Chellappan, R.K.; Foix, D.; Krajnc, A.; Mali, G.; Drazic, G.; Genorio, B.; Dedryvère, R.; Dominko, R. Fluorinated reduced graphene oxide as an interlayer in Li–S batteries. *Chem. Mater.* **2015**, *27*, 7070–7081. [[CrossRef](#)]
69. Lei, T.; Lei, T.; Chen, W.; Lv, W.; Huang, J.; Zhu, J.; Chu, J.; Yan, C.; Wu, C.; Yan, Y.; et al. Inhibiting polysulfide shuttling with a graphene composite separator for highly robust lithium–sulfur batteries. *Joule* **2018**, *2*, 2091–2104. [[CrossRef](#)]
70. Zhao, Y.; Gu, Z.; Weng, W.; Zhou, D.; Liu, Z.; Fan, W.; Deng, S.; He, H.; Yao, X. Nitrogen doped hollow carbon nanospheres as efficient polysulfide restricted layer on commercial separators for high-performance lithium-sulfur batteries. *Chinese Chem. Lett.* **2023**, *34*, 107232. [[CrossRef](#)]
71. Wu, P.; Hu, H.-Y.; Xie, N.; Wang, C.; Wu, F.; Pan, M.; Li, H.-F.; Wang, X.-D.; Zeng, Z.; Deng, S.; et al. A N-doped graphene-cobalt nickel sulfide aerogel as a sulfur host for lithium–sulfur batteries. *RSC Adv.* **2019**, *9*, 32247–32257. [[CrossRef](#)]
72. Li, Y.; Fan, J.; Zhang, J.; Yang, J.; Yuan, R.; Chang, J.; Zheng, M.; Dong, Q. A honeycomb-like Co@N–C composite for ultrahigh sulfur loading Li–S batteries. *ACS Nano* **2017**, *11*, 11417–11424. [[CrossRef](#)] [[PubMed](#)]
73. Li, Z.; Jiang, Y.; Yuan, L.; Yi, Z.; Wu, C.; Liu, Y.; Strasser, P.; Huang, Y. A highly ordered meso@microporous carbon-supported sulfur@smaller sulfur core–shell structured cathode for Li–S batteries. *ACS Nano* **2014**, *8*, 9295–9303. [[CrossRef](#)] [[PubMed](#)]
74. Wu, P.; Tan, L.; Wang, X.D.; Liao, P.; Liu, Z.; Hou, P.P.; Zhou, Q.Y.; Jin, X.J.; Chao, M.; Shao, X.R.; et al. Porous 3D nitrogen-doped rGO/Co–Ni–S composite modified separator for high-capacity and stable lithium–sulfur batteries. *Mater. Res. Bull.* **2022**, *145*, 111550. [[CrossRef](#)]
75. Fang, R.; Zhao, S.; Pei, S.; Qian, X.; Hou, P.-X.; Cheng, H.-M.; Liu, C.; Li, F. Toward more reliable lithium–sulfur batteries: An all-graphene cathode structure. *ACS Nano* **2016**, *10*, 8676–8682. [[CrossRef](#)] [[PubMed](#)]
76. Díez, N.; Sevilla, M.; Fuertes, A.B. N/S–Co-doped porous carbon nanoparticles serving the dual function of sulfur host and separator coating in lithium–sulfur batteries. *ACS Appl. Energy Mater.* **2020**, *3*, 3397–3407. [[CrossRef](#)]
77. Song, X.; Wang, S.; Chen, G.; Gao, T.; Bao, Y.; Ding, L.X.; Wang, H. Fe–N-doped carbon nanofiber and graphene modified separator for lithium–sulfur batteries. *Chem. Eng. J.* **2018**, *333*, 564–571. [[CrossRef](#)]
78. Zhang, Z.; Lai, Y.; Zhang, Z.; Zhang, K.; Li, J. Al<sub>2</sub>O<sub>3</sub>-coated porous separator for enhanced electrochemical performance of lithium sulfur batteries. *Electrochim. Acta* **2014**, *129*, 55–61. [[CrossRef](#)]
79. Han, H.; Niu, S.; Zhao, Y.; Tan, T.; Zhang, Y. TiO<sub>2</sub>/porous carbon composite-decorated separators for lithium/sulfur battery. *Nanoscale Res. Lett.* **2019**, *14*, 176. [[CrossRef](#)]
80. Gao, Z.; Xue, Z.; Miao, Y.; Chen, B.; Xu, J.; Shi, H.; Tang, T.; Zhao, X. TiO<sub>2</sub>@Porous carbon nanotubes modified separator as polysulfide barrier for lithium–sulfur batteries. *J. Alloy. Compd.* **2022**, *906*, 164249. [[CrossRef](#)]
81. Li, J.; Huang, Y.; Zhang, S.; Jia, W.; Wang, X.; Guo, Y.; Jia, D.; Wang, L. Decoration of silica nanoparticles on polypropylene separator for lithium–sulfur batteries. *ACS Appl. Mater. Interfaces* **2017**, *9*, 7499–7504. [[CrossRef](#)] [[PubMed](#)]
82. Liu, D.; Zhang, C.; Zhou, G.; Lv, W.; Ling, G.; Zhi, L.; Yang, Q.H. Catalytic effects in lithium–sulfur batteries: Promoted sulfur transformation and reduced shuttle effect. *Adv. Sci.* **2018**, *5*, 1700270. [[CrossRef](#)] [[PubMed](#)]
83. Li, S.; Cen, Y.; Xiang, Q.; Aslam, M.K.; Hu, B.; Li, W.; Tang, Y.; Yu, Q.; Liu, Y.; Chen, C. Vanadium dioxide-reduced graphene oxide binary host as an efficient polysulfide plague for high-performance lithium–sulfur batteries. *J. Mater. Chem.* **2019**, *7*, 1658–1668. [[CrossRef](#)]
84. Yuan, H.; Peng, H.J.; Li, B.Q.; Xie, J.; Kong, L.; Zhao, M.; Chen, X.; Huang, J.Q.; Zhang, Q. Conductive and catalytic triple-phase interfaces enabling uniform nucleation in high-rate lithium–sulfur batteries. *Adv. Energy Mater.* **2019**, *9*, 1802768. [[CrossRef](#)]
85. Qian, X.; Zhao, D.; Jin, L.; Shen, X.; Yao, S.; Rao, D.; Zhou, Y.; Xi, X.M. Hollow spherical Lanthanum oxide coated separator for high electrochemical performance lithium–sulfur batteries. *Mater. Res. Bull.* **2017**, *94*, 104–112. [[CrossRef](#)]
86. Tan, L.; Li, X.; Wang, Z.; Guo, H.; Wang, J. Lightweight reduced graphene Oxide@MoS<sub>2</sub> interlayer as polysulfide barrier for high-performance lithium–sulfur batteries. *ACS Appl. Mater. Interfaces* **2018**, *10*, 3707–3713. [[CrossRef](#)]

87. Fan, H.J.; Knez, M.; Scholz, R.; Nielsch, K.; Pippel, E.; Hesse, D.; Zacharias, M.; Gösele, U. Monocrystalline spinel nano-tube fabrication based on the Kirkendall effect. *Nat. Mater.* **2006**, *5*, 627–631. [[CrossRef](#)]
88. Zheng, N.; Jiang, G.; Chen, X.; Mao, J.; Jiang, N.; Li, Y. Battery separators functionalized with edge-rich MoS<sub>2</sub>/C hollow microspheres for the uniform deposition of Li<sub>2</sub>S in high-performance lithium–sulfur batteries. *Nano-Micro Lett.* **2019**, *11*, 43. [[CrossRef](#)]
89. Mao, L.; Mao, J. Ultralow-decay lithium–sulfur batteries: Modified separator with graphene/ZnS(en)<sub>0.5</sub> exfoliation nanosheets. *J. Solid State Chem.* **2020**, *290*, 121555. [[CrossRef](#)]
90. Yao, W.; Zheng, W.; Xu, J.; Tian, C.; Han, K.; Sun, W.; Xiao, S. ZnS-SnS@NC Heterostructure as robust lithiophilicity and sulfiphilicity mediator toward high-rate and long-life lithium–sulfur batteries. *ACS Nano* **2021**, *15*, 7114–7130. [[CrossRef](#)]
91. Wang, G.; Jiao, Q.; Zhang, Z.; Zhao, Y.; Lin, C.; Zhang, X.; Ma, H.; Dai, S.; Xu, T. Improved electrochemical behavior of Li–S battery with functional WS<sub>2</sub>@PB–PPy–modified separator. *Chem. Eng. J. Adv.* **2021**, *8*, 100145. [[CrossRef](#)]
92. Xiao, Y.; Hwang, J.Y.; Sun, Y.K. Transition metal carbide-based materials: Synthesis and applications in electrochemical energy storage. *J. Mater. Chem. A* **2016**, *4*, 10379–10393. [[CrossRef](#)]
93. Cui, Z.; Yao, J.; Mei, T.; Zhou, S.; Hou, B.; Li, J.; Li, J.; Wang, J.; Qian, J.; Wang, X. Strong lithium polysulfides chemical trapping of TiC–TiO<sub>2</sub>/S composite for long-cycle lithium–sulfur batteries. *Electrochim. Acta* **2019**, *298*, 43–51. [[CrossRef](#)]
94. Zhang, Y.; Zhang, P.; Li, B.; Zhang, S.; Liu, K.; Hou, R.; Zhang, X.; Silva, S.R.; Shao, G. Vertically aligned graphene nanosheets on multi-yolk/shell structured TiC@C nanofibers for stable Li–S batteries. *Energy Storage Mater.* **2020**, *27*, 159–168. [[CrossRef](#)]
95. Liu, S.; Luo, J.; Xiong, Y.; Chen, Z.; Zhang, K.; Rui, G.; Wang, L.; Hu, G.; Jiang, J.; Mei, T. Taming polysulfides in an Li–S battery with low-temperature one-step chemical synthesis of titanium carbide nanoparticles from waste PTFE. *Front. Chem.* **2021**, *9*, 638557. [[CrossRef](#)]
96. Zhao, J.; Yan, Z. Flexible TiC modified separators trapping polysulfide for high performance lithium–sulfur batteries. *J. Alloys Compd.* **2021**, *856*, 156609. [[CrossRef](#)]
97. Moon, S.-H.; Kim, J.-H.; Shin, J.-H.; Jang, J.-S.; Kim, S.-B.; Lee, S.-N.; Kwon, S.-H.; Park, K.-W. High absorption and fast polysulfides conversion of dual functional separator based on mesoporous-WC/rGO composite for lithium–sulfur batteries. *J. Alloy. Compd.* **2022**, *904*, 164120. [[CrossRef](#)]
98. Zhao, P.; Zhang, Z.; He, H.; Yu, Y.; Li, X.; Xie, W.; Yang, Z.; Cai, J. Cobalt-tungsten bimetallic carbide nanoparticles as efficient catalytic material for high-performance lithium–sulfur batteries. *ChemSusChem* **2019**, *12*, 4866–4873. [[CrossRef](#)]
99. Cai, W.; Li, G.; Zhang, K.; Xiao, G.; Wang, C.; Ye, K.; Chen, Z.; Zhu, Y.; Qian, Y. Conductive nanocrystalline niobium carbide as high efficiency polysulfides tamer for lithium–sulfur batteries. *Adv. Funct. Mater.* **2017**, *28*, 1704865. [[CrossRef](#)]
100. Abghoui, Y.; Skúlason, E. Transition Metal Nitride Catalysts for Electrochemical Reduction of Nitrogen to Ammonia at Ambient Conditions. *Procedia Computer Sci.* **2015**, *51*, 1897–1906. [[CrossRef](#)]
101. Lan, L.; Chen, D.; Yao, Y.; Peng, X.; Wu, J.; Li, Y.; Ping, J.; Ying, Y. Phase-dependent fluorescence quenching efficiency of MoS<sub>2</sub> nanosheets and their applications in multiplex target biosensing. *ACS Appl. Mater. Interfaces* **2018**, *10*, 42009–42017. [[CrossRef](#)] [[PubMed](#)]
102. Chen, G.; Song, X.; Wang, S.; Chen, X.; Wang, H. Two dimensional molybdenum nitride nanosheets modified Celgard separator with multifunction for Li–S batteries. *J. Power Sources* **2018**, *408*, 58–64. [[CrossRef](#)]
103. Kim, H.S.; Kang, H.J.; Lim, H.; Hwang, H.J.; Park, J.W.; Lee, T.G.; Cho, S.Y.; Jang, S.G.; Jun, Y.S. Boron nitride nanotube-based separator for high-performance lithium–sulfur batteries. *Nanomaterials* **2022**, *12*, 11. [[CrossRef](#)] [[PubMed](#)]
104. Chen, Y.; Kang, Q.; Jiang, P.; Huang, X. Rapid, high-efficient and scalable exfoliation of high-quality boron nitride nanosheets and their application in lithium–sulfur batteries. *Nano Res.* **2021**, *14*, 2424–2431. [[CrossRef](#)]
105. Luo, M.; Bai, Y.; Sun, R.; Wang, Z.; Sun, W.; Lin, P.; Dai, X.; Sun, K. Enhanced performance of lithium–sulfur batteries with Co-doped g-C<sub>3</sub>N<sub>4</sub> nanosheet-based separator. *Ind. Eng. Chem. Res.* **2021**, *60*, 1231–1240. [[CrossRef](#)]
106. Huang, S.; Huixiang, E.; Yang, Y.; Zhang, Y.; Ye, M.; Li, C.C. Transition metal phosphides: New generation cathode host/separator modifier for Li–S batteries. *J. Mater. Chem. A* **2021**, *9*, 7458–7480. [[CrossRef](#)]
107. Chen, X.; Ding, X.; Wang, C.; Feng, Z.; Xu, L.; Gao, X.; Zhai, Y.; Wang, D. A multi-shelled CoP nanosphere modified separator for highly efficient Li–S batteries. *Nanoscale* **2018**, *10*, 13694–13701. [[CrossRef](#)]
108. Lin, J.; Zhang, K.; Zhu, Z.; Zhang, R.; Li, N.; Zhao, C. CoP/C nanocubes-modified separator suppressing polysulfide dissolution for high-rate and stable lithium–sulfur batteries. *ACS Appl. Mater. Interfaces* **2019**, *12*, 2497–2504. [[CrossRef](#)]
109. Zhao, Z.; Li, H.; Cheng, X.; Ren, R.; Meng, Z.; Wang, X. Multifunctional FeP/spongy carbon modified separator with enhanced polysulfide immobilization and conversion for flame-retardant lithium–sulfur batteries. *Chem. Select* **2021**, *6*, 7098–7102. [[CrossRef](#)]
110. Mao, J.; Niu, D.; Huang, G.; Jin, X.; Wei, C.; Cai, J.; Li, Y.; Shi, J. A Ni/Ni<sub>2</sub>P heterostructure in modified porous carbon separator for boosting polysulfide catalytic conversion. *Sci. China Mater.* **2022**, *65*, 2453–2462. [[CrossRef](#)]
111. Zhou, G.; Tian, H.; Jin, Y.; Tao, X.; Liu, B.; Zhang, R.; Seh, Z.W.; Zhuo, D.; Liu, Y.; Sun, J.; et al. Catalytic oxidation of Li<sub>2</sub>S on the surface of metal sulfides for Li–S batteries. *PNAS* **2017**, *114*, 840–845. [[CrossRef](#)]
112. Peng, H.J.; Zhang, G.; Chen, X.; Zhang, Z.W.; Xu, W.T.; Huang, J.Q.; Zhang, Q. Enhanced electrochemical kinetics on conductive polar mediators for lithium–sulfur batteries. *Angew. Chem. Int. Ed.* **2016**, *55*, 12990–12995. [[CrossRef](#)] [[PubMed](#)]
113. Liu, Y.; Chen, C.; Valdez, J.; Motta Meira, D.; He, W.; Wang, Y.; Harnagea, C.; Lu, Q.; Guner, T.; Wang, H.; et al. Phase-enabled metal-organic framework homojunction for highly selective CO<sub>2</sub>. *Photoreduction. Nat. Comm.* **2021**, *12*, 1231. [[CrossRef](#)] [[PubMed](#)]

114. Peng, Y.; Li, Y.; Ban, Y.; Jin, H.; Jiao, W.; Liu, X.; Yang, W. Metal-organic framework nanosheets as building blocks for molecular sieving membranes. *Science* **2014**, *346*, 1356–1359. [[CrossRef](#)]
115. Wang, B.; Cote, A.P.; Furukawa, H.; O’Keeffe, M.; Yaghi, O.M. Colossal cages in zeolitic imidazolate frameworks as selective carbon dioxide reservoirs. *Nature* **2008**, *453*, 207–211. [[CrossRef](#)]
116. Bai, S.; Sheng, T.; Tan, C.; Zhu, Q.; Huang, Y.; Jiang, H.; Hu, S.; Fu, R.; Wu, X. Distinct anion sensing by a 2D self-assembled Cu(I)-based metal–organic polymer with versatile visual colorimetric responses and efficient selective separations via anion exchange. *J. Mater. Chem. A* **2013**, *1*, 2970. [[CrossRef](#)]
117. Mori, R. Cathode materials for lithium–sulfur battery: A review. *J. Solid State Electrochem.* **2023**, *27*, 813–839. [[CrossRef](#)]
118. Bai, S.; Liu, X.; Zhu, K.; Wu, S.; Zhou, H. Metal-organic framework-based separator for lithium–sulfur batteries. *Nat. Energy* **2016**, *1*, 16094. [[CrossRef](#)]
119. Dang, B.; Li, Q.; Luo, Y.; Zhao, R.; Li, J.; Wu, F. Metal-organic framework-based glass fiber separator as an efficacious polysulfide barrier and dendrite suppressor for lithium–sulfur batteries. *J. Alloys Compd.* **2022**, *915*, 165375. [[CrossRef](#)]
120. Su, Y.; Wang, W.; Wang, W.; Wang, A.; Huang, Y.; Guan, Y. Cerium-based MOF as a separator coating for high-performance lithium–sulfur batteries. *J. Electrochem. Soc.* **2022**, *169*, 030528. [[CrossRef](#)]
121. Ma, B.; Zhang, X.; Deng, X.; Huang, S.; Xiao, M.; Wang, S.; Han, D.; Meng, Y. Construction of KB@ZIF-8/PP composite separator for lithium–sulfur batteries with enhanced electrochemical performance. *Polymers* **2021**, *13*, 4210. [[CrossRef](#)]
122. Baker, S.N.; Baker, G.A. Luminescent carbon nanodots: Emergent nanolights. *Angew. Chem. Int. Ed.* **2010**, *49*, 6726–6744. [[CrossRef](#)]
123. Fowley, C.; Nomikou, N.; McHale, A.P.; McCaughan, B.; Callan, J.F. Extending the tissue penetration capability of conventional photosensitisers: A carbon quantum dot–protoporphyrin IX conjugate for use in two-photon excited photodynamic therapy. *Chem Commun (Camb)* **2013**, *49*, 8934–8936. [[CrossRef](#)]
124. Xu, Q.; Niu, Y.; Li, J.; Yang, Z.; Gao, J.; Ding, L.; Ni, H.; Zhu, P.; Liu, Y.; Tang, Y.; et al. Recent progress of quantum dots for energy storage applications. *Carbon. Neutrality* **2022**, *1*, 13. [[CrossRef](#)]
125. Ding, H.; Zhang, Q.; Liu, Z.; Wang, J.; Ma, R.; Fan, L.; Wang, T.; Zhao, J.; Ge, J.; Lu, X.; et al. TiO<sub>2</sub> quantum dots decorated multi-walled carbon nanotubes as the multifunctional separator for highly stable lithium sulfur batteries. *Electrochim. Acta* **2018**, *284*, 314–320. [[CrossRef](#)]
126. Pang, Y.; Wei, J.; Wang, Y.; Xia, Y. Synergetic protective effect of the ultralight MWCNTs/NCQDs modified separator for highly stable lithium–sulfur batteries. *Adv. Energy Mater.* **2018**, *8*, 1702288. [[CrossRef](#)]
127. Chung, S.H.; Manthiram, A. High-performance Li–S batteries with an ultra-lightweight MWCNT-coated separator. *J. Phys. Chem. Lett.* **2014**, *5*, 197. [[CrossRef](#)] [[PubMed](#)]
128. Yu, B.; Chen, D.; Wang, Z.; Qi, F.; Zhang, X.; Wang, X.; Hu, Y.; Wang, B.; Zhang, W.; Chen, Y.; et al. Mo<sub>2</sub>C quantum dots@graphene functionalized separator toward high-current-density lithium metal anodes for ultrastable Li–S batteries. *Chem. Eng. J.* **2020**, *399*, 125837. [[CrossRef](#)]
129. Liu, Z.; Hu, Z.; Jiang, X.; Zhang, Y.; Wang, X.; Zhang, S. Multi-functional ZnS quantum Dots/Graphene aerogel modified separator for high performance lithium–sulfur batteries. *Electrochim. Acta* **2022**, *422*, 140496. [[CrossRef](#)]
130. Zhang, J.; Cheng, Y.; Chen, H.; Wang, Y.; Chen, Q.; Hou, G.; Wen, M.; Tang, Y. MoP quantum dot-modified N,P-carbon nanotubes as a multifunctional separator coating for high-performance lithium–sulfur batteries. *ACS Appl. Mater. Interfaces* **2022**, *14*, 16289–16299. [[CrossRef](#)]
131. Liu, Q.; Han, X.; Park, H.; Kim, J.; Xiong, P.; Yuan, H.; Yeon, J.S.; Kang, Y.; Park, J.M.; Dou, Q.; et al. Layered double hydroxide quantum dots for use in a bifunctional separator of lithium–sulfur batteries. *ACS Appl. Mater. Interfaces* **2021**, *13*, 179780. [[CrossRef](#)] [[PubMed](#)]
132. Ran, J.R.; Gao, G.; Li, F.T.; Ma, T.Y.; Du, A.; Qiao, S.Z. Ti<sub>3</sub>C<sub>2</sub> MXene co-catalyst on metal sulfide photo-absorbers for enhanced visible-light photocatalytic hydrogen production. *Nat. Commun.* **2017**, *8*, 13907. [[CrossRef](#)] [[PubMed](#)]
133. Zhao, S.S.; Meng, X.; Zhu, K.; Du, F.; Chen, G.; Wei, Y.J.; Gogotsi, Y.; Gao, Y. Li-ion uptake and increase in interlayer spacing of Nb<sub>4</sub>C<sub>3</sub> MXene. *Energy Storage Mater.* **2017**, *8*, 42–48. [[CrossRef](#)]
134. Naguib, M.; Kurtoglu, M.; Presser, V.; Lu, J.; Niu, J.; Heon, M.; Hultman, L.; Gogotsi, Y.; Barsoum, M.W. Two-dimensional nanocrystals produced by exfoliation of Ti<sub>3</sub>AlC<sub>2</sub>. *Adv. Mater.* **2011**, *23*, 4248–4253. [[CrossRef](#)] [[PubMed](#)]
135. Lukatskaya, M.R.; Mashtalir, O.; Ren, C.E.; Dall’agnese, Y.; Rozier, P.; Taberna, P.L.; Naguib, M.; Simon, P.; Barsoum, M.W.; Gogotsi, Y. Cation intercalation and high volumetric capacitance of two-dimensional titanium carbide. *Science* **2013**, *341*, 1502–1505. [[CrossRef](#)]
136. Er, D.; Li, J.; Naguib, M.; Gogotsi, Y.; Shenoy, V.B. Ti<sub>3</sub>C<sub>2</sub> MXene as a high capacity electrode material for metal (Li, Na, K, Ca) ion batteries. *ACS Appl. Mater. Interfaces* **2014**, *6*, 11173–11179. [[CrossRef](#)]
137. Naguib, M.; Mochalin, V.N.; Barsoum, M.W.; Gogotsi, Y. 25th anniversary article: MXenes: A new family of two-dimensional materials. *Adv. Mater.* **2014**, *26*, 992–1005. [[CrossRef](#)]
138. Saeed, M.A.; Shahzad, A.; Rasool, K.; Mateen, F.; Oh, J.; Shim, J.W. 2D MXene: A potential candidate for photovoltaic cells? a critical review. *Adv. Sci.* **2020**, *9*, 2104743. [[CrossRef](#)]
139. Chen, X.; Shi, Z.; Tian, Y.; Lin, P.; Wu, D.; Li, X.; Dong, B.; Xu, W.; Fang, X. Two-dimensional Ti<sub>3</sub>C<sub>2</sub> MXene-based nanostructures for emerging optoelectronic applications. *Mater. Horiz.* **2021**, *8*, 2929–2963. [[CrossRef](#)]

140. Wojciechowski, T.; Rozmysłowska-Wojciechowska, A.; Matyszczak, G.; Wrzeczonek, M.; Olszyna, A.; Peter, A.; Mihaly-Cozmuta, A.; Nicula, C.; Mihaly-Cozmuta, L.; Podsiadło, S.; et al. Ti<sub>2</sub>C MXene modified with ceramic oxide and noble metal nanoparticles: Synthesis, morphostructural properties, and high photocatalytic activity. *Inorg. Chem.* **2019**, *58*, 7602–7614. [[CrossRef](#)]
141. Gao, L.; Chen, H.; Kuklin, A.V.; Wageh, S.; Al-Ghamdi, A.A.; Ågren, H.; Zhang, H. Optical properties of few-layer Ti<sub>3</sub>CN MXene: From experimental observations to theoretical calculations. *ACS Nano* **2022**, *16*, 3059–3069. [[CrossRef](#)] [[PubMed](#)]
142. Naguib, M.; Mashtali, O.; Carle, J.; Presser, V.; Lu, J.; Hultman, L.; Gogotsi, Y.; Barsoum, M.W. Two-dimensional transition metal carbides. *ACS Nano* **2012**, *6*, 1322–1331. [[CrossRef](#)] [[PubMed](#)]
143. Lin, C.; Zhang, W.; Wang, L.; Wang, Z.; Zhao, W.; Duan, W.; Zhao, Z.; Liu, B.; Jin, J. A few-layered Ti<sub>3</sub>C<sub>2</sub> nanosheet/glass fiber composite separator as a lithium polysulphide reservoir for high-performance lithium–sulfur batteries. *J. Mater. Chem.* **2016**, *4*, 5993–5998. [[CrossRef](#)]
144. Jiao, L.; Zhang, C.; Geng, C.; Wu, S.; Li, H.; Lv, W.; Tao, Y.; Chen, Z.; Zhou, G.; Li, J.; et al. Capture and catalytic conversion of polysulfides by in situ built TiO<sub>2</sub>-MXene heterostructures for lithium–sulfur batteries. *Adv. Energy Mater.* **2019**, *9*, 190021. [[CrossRef](#)]
145. Yao, Y.; Wang, S.; Jia, X.; Yang, J.; Li, Y.; Liao, J.; Song, H. Freestanding sandwich-like hierarchically TiS<sub>2</sub>-TiO<sub>2</sub>/MXene bi-functional interlayer for stable Li–S batteries. *Carbon* **2022**, *188*, 533–542. [[CrossRef](#)]
146. Li, P.; Lv, H.; Li, Z.; Meng, X.; Lin, Z.; Wang, R.; Li, X. The Electrostatic Attraction and Catalytic Effect Enabled by Ionic-Covalent Organic Nanosheets on MXene for Separator Modification of Lithium–Sulfur Batteries. *Adv. Mater.* **2021**, *33*, 2007803. [[CrossRef](#)]
147. Wang, J.; Zhai, P.; Zhao, T.; Li, M.; Yang, Z.; Zhang, H.; Huang, J. Lamina MXene-Nafion-modified separator with highly inhibited shuttle effect for long-life lithium–sulfur batteries. *Electrochimica Acta* **2019**, *320*, 134558. [[CrossRef](#)]
148. He, Y.; Qiao, Y.; Chang, Z.; Cao, X.; Jia, M.; He, P.; Zhou, H. Developing A “polysulfide-phobic” strategy to restrain shuttle effect in lithium–sulfur batteries. *Angew. Chem. Int. Ed.* **2019**, *58*, 11774–11778. [[CrossRef](#)]
149. Huang, J.Q.; Zhang, Q.; Peng, H.J.; Liu, X.Y.; Qian, W.Z.; Wei, F. Ionic shield for polysulfides towards highly-stable lithium–sulfur batteries. *Energy Environ. Sci.* **2013**, *7*, 347–353. [[CrossRef](#)]
150. Zhang, Z.; Yi, S.; Wei, Y.; Bian, H.; Wang, R.; Min, Y. Lignin nanoparticle-coated celgard separator for high-performance lithium–sulfur batteries. *Polymers* **2019**, *11*, 1946. [[CrossRef](#)]
151. Henriksson, M.; Berglund, L.A.; Isaksson, P.; Lindstrom, T.; Nishino, T. Cellulose nanopaper structures of high toughness. *Biomacromolecules* **2008**, *9*, 1579–1585. [[CrossRef](#)] [[PubMed](#)]
152. Pavlin, N.; Hribernik, S.; Kapun, G.; Talian, S.D.; Njel, C.; Dedryvère, R.; Dominko, R. The role of cellulose based separator in lithium sulfur batteries. *J. Electrochem. Soc.* **2019**, *166*, A5237–A5243. [[CrossRef](#)]
153. Tian, Y.W.; Zhang, Y.J.; Wu, L.; Dong, W.D.; Huang, R.; Dong, P.Y.; Yan, M.; Liu, J.; Mohamed, H.S.H.; Chen, L.H.; et al. Bifunctional Separator with Ultra-Lightweight MnO<sub>2</sub> Coating for Highly Stable Lithium–Sulfur Batteries. *ACS Appl. Mater. Interfaces* **2023**, *15*, 6877–6887. [[CrossRef](#)] [[PubMed](#)]
154. Chen, K.; Li, Y.; Zhan, H. Advanced separators for lithium-ion batteries. *IOP Conf. Ser. Earth Environ. Sci.* **2022**, *1011*, 012009. [[CrossRef](#)]
155. Huang, X. Separator technologies for lithium-ion batteries. *J. Solid. State Electrochem.* **2011**, *15*, 649–662. [[CrossRef](#)]
156. Deimede, V.; Elmasides, C. Separators for lithium-ion batteries: A review on the production processes and recent developments. *Energy Technol.* **2015**, *3*, 453–468. [[CrossRef](#)]
157. Zhang, L.; Li, X.; Yang, M.; Chen, W. High-safety separators for lithium-ion batteries and sodium-ion batteries: Advances and perspective, energy storage materials. *ScienceDirect* **2021**, *41*, 522–545.
158. Lee, H.; Yanilmaz, M.; Toprakci, O.; Fu, K.; Zhang, X. A review of recent developments in membrane separators for rechargeable lithium-ion batteries. *Energy Environ. Sci.* **2014**, *7*, 3857–3886. [[CrossRef](#)]
159. Francis, C.F.J.; Kyratzis, I.L.; Best, A.S. Lithium-ion battery separators for ionic-liquid. electrolytes: A review. *Adv. Mater.* **2020**, *32*, 1904205. [[CrossRef](#)]
160. Xie, Y.; Zou, H.; Xiang, H.; Xia, R.; Liang, D.; Shi, P.; Dai, S.; Wang, H. Enhancement on the wettability of lithium battery separator toward nonaqueous electrolytes. *J. Membr. Sci.* **2016**, *503*, 25–30. [[CrossRef](#)]
161. Mori, R.; Yokokawa, K. Silicon Coupling Agent Treatment of Cathode Material for Lithium Sulfur Battery. JP Patent No. 2022-155874, 14 October 2022.

**Disclaimer/Publisher’s Note:** The statements, opinions and data contained in all publications are solely those of the individual author(s) and contributor(s) and not of MDPI and/or the editor(s). MDPI and/or the editor(s) disclaim responsibility for any injury to people or property resulting from any ideas, methods, instructions or products referred to in the content.